- 1 The Dynamic Influence of Subsurface Geological Processes on the Assembly and
- 2 Diversification of Thermophilic Microbial Communities in Continental Hydrothermal
- 3 Systems.
- 4 Kenneth W.W. Sims^{1,2*}, Cole M. Messa^{1,2}, Sean R. Scott^{1,2}, Andrew D. Parsekian^{2,3}, Andrew
- 5 Miller^{1,2}, Abraham L. Role^{1,2}, Timothy P. Moloney^{1,2}, Everett L. Shock ^{4,5}, Jacob B. Lowenstern⁶,
- 6 R. Blaine McCleskey⁷, Mathew A. Charette⁸, Bradley J. Carr², Sylvain Pasquet ^{2, 9, 10}, Henry
- 7 Heasler¹¹, Cheryl Jaworowoski¹¹, W. Steven Holbrook^{2, 12}, Melody R. Lindsay¹³, Daniel R.
- 8 Colman¹³, Eric S. Boyd¹³
- 9 1) University of Wyoming High Precision Isotope Laboratory, University of Wyoming,
- 10 Laramie, WY, USA
- 11 2) Department of Geology and Geophysics, University of Wyoming, Laramie, WY, USA
- 12 3) Department of Civil & Architectural Engineering, University of Wyoming, Laramie, WY,
- 13 USA
- 14 4) School of Molecular Sciences, Arizona State University, Tempe, AZ, USA
- 15 School of Earth and Space Exploration, Arizona State University, Tempe, AZ USA
- 16 6) United States Geological Survey, Vancouver, WA, USA
- 17 7) United States Geological Survey, Boulder, CO, USA
- 18 8) Department of Chemistry and Geochemistry, Woods Hole Oceanographic Institution, Woods
- 19 Hole, MA, USA
- 20 9) UAR 3455 OSU ECCE TERRA, CNRS, Sorbonne Université, 75005 Paris, France
- 21 10) UMR 7619 METIS, CNRS, Sorbonne Université, EPHE, 75005 Paris, France
- 22 11) National Park Service, Mammoth, Wyoming, USA
- 23 12) Department of Geosciences, Virginia Tech, Blacksburg, VA, USA
- 24 13) Department of Microbiology and Cell Biology, Montana State University, Bozeman, MT,
- 25 USA
- * Corresponding Author (ksims7@uwyo.edu)

28 An accepted paradigm of hydrothermal systems is the process of phase separation, or boiling, 29 of a deep, homogeneous hydrothermal fluid as it ascends through the subsurface resulting in 30 gas rich and gas poor fluids. While phase separation helps to explain first-order patterns in 31 the chemistry and biology of a hot spring's surficial expression, we know little about the subsurface architecture beneath "phase-separated" pools and the timescales over which phase 32 33 separation processes occur. Essentially, we have a two-dimensional understanding of a four-34 dimensional process. By combining geophysical, geochemical, isotopic, and microbiological 35 measurements of two adjacent phase-separated hot springs in Norris Geyser Basin, Yellowstone National Park, we provide a four-dimensional assessment of phase separation 36 37 processes and their biological manifestation. We uniquely show that Yellowstone's 38 hydrothermal waters originate from a deep sedimentary aquifer and that both meteoric 39 recharge and shallow reactive transport processes are required to establish the geobiological 40 feedbacks that drive bimodal distributions in the geochemical and microbial composition of 41 hot springs. Specifically, over periods of tens of years, gas-enriched fluids containing volcanic 42 sulfide mix with meteoric waters resulting in microbially-mediated production of sulfuric acid 43 by thermoacidophilic Archaea in the near subsurface. In contrast, over periods of hundreds of 44 years, anoxic residual liquid rises to the surface where it is infused with atmospheric gas 45 fostering Archaea and Bacteria that are largely dependent on oxygen. As such, our results provide formative insight into the causative links between subsurface geological processes, the 46 47 development of geochemical fluids, and the assembly and diversification of thermophilic 48 microbial communities in hydrothermal systems.

49

- 50 Keywords: Hydrothermal Systems, Reactive Transport, Phase Separation, Timescales of
- 51 Water-Rock Interaction, Thermophilic Microbial Communities, Yellowstone, U- and Th-
- 52 Decay Series, Radiogenic Isotopes, Near Surface Geophysics.

53

54

55

56

57

58

59

60

61

62

1. INTRODUCTION

Hydrothermal systems have been common since early in Earth history, form on timescales of minutes to thousands of years, are products of significant heat and mass transfer, and support diverse microbial communities. However, our understanding of how subsurface geological processes, such as reactive transport, phase separation, and shallow groundwater mixing, control hot spring geochemistry and in turn support microbial ecosystems and drive microbial diversification is poorly understood.

Yellowstone's hydrothermal system (hereafter referred to as Yellowstone) hosts the world's largest and most profound example of an active continental hydrothermal system with a

- surface expression (Hague, 1904; Allen and Day, 1935; White, 1957; Hurwitz and Lowenstern,
- 64 2014). A first-order observation of Yellowstone hydrothermal waters is that they have a distinct
- 65 bimodal distribution of pH (Allen and Day, 1935; White, 1957; Fournier, 1989; Nordstrom et al.,
- 2009; Lowenstern et al., 2012; Hurwitz and Lowenstern, 2014). To explain this bimodal
- distribution in the pH of Yellowstone hydrothermal waters, decades of research (White, 1957;
- 68 Fournier, 1989; Nordstrom et al., 2009) have led to a simple and rather elegant model known as
- 69 "phase separation." At its simplest, the model implies that a deep, hydrothermal reservoir,
- recharged by meteoric water and infused with crustal and magmatic gases, underlies all of
- Yellowstone (Rye and Truesdell, 1993, 2007; Kharaka et al., 2002). Heat-induced pressure and
- density differences provide driving forces that cause the deep hydrothermal fluids to ascend to
- 73 the surface along high-permeability pathways, such as fractures and faults. Decompression
- boiling of the fluid ascending from the deep reservoir results in physical separation of a low-
- density vapor phase (made dominantly of steam, >>90%, and trace non-condensable gases) and a
- denser liquid phase (made dominantly of water, with non-volatile, soluble anions and cations).
- 77 The model holds that the two phases diverge and then migrate to the surface along different
- 78 flow-paths. Fluids derived from the separated liquid tend to be near neutral to moderately basic
- and maintain their full inheritance of chloride (Cl⁻), as this ion is unlikely to partition into the
- 80 vapor phase. These alkaline-chloride hydrothermal fluids also precipitate silica sinter that armors
- 81 their flow-paths against water-rock interaction. In contrast, the vapor phase input (>>90% steam)
- 82 is depleted in Cl⁻ and enriched in volatile trace gases such as hydrogen sulfide (H₂S)
- 83 (Lowenstern et al., 2012). Subsequent mixing of the vapor phase with infiltrating, oxidizing,
- oxygen-rich near-surface groundwater (Fournier, 1989; W. Payton Gardner et al., 2010; Hurwitz
- and Lowenstern, 2014) converts the trace gas H₂S and its derivatives (i.e., native sulfur (S⁰) and
- sulfide minerals) to SO₄². These distinct water types have also been shown to host
- 87 taxonomically and functionally dissimilar biological communities. High temperature acid-sulfate
- springs are dominated by aerobic Archaea (Inskeep et al., 2013; Ward et al., 2017; Colman et al.,
- 89 2018) and their communities are enriched in functionalities that further facilitate the
- 90 dissimilation and oxidation of sulfur compounds, thereby enhancing the water's acidity (Mosser
- et al., 1973; Colman et al., 2018, 2019). In contrast, high temperature alkaline-chloride
- 92 communities include both aerobic and anaerobic archaeal and bacterial members (Inskeep et al.,
- 93 2013; Ward et al., 2017; Colman et al., 2018; Fernandes-Martins et al., 2021) that display a

variety of metabolic strategies that are less dependent on dissimilatory metabolism of sulfur compounds and possibly more dependent on arsenic compounds (Fernandes-Martins et al., 2021).

While this first-order geochemical and hydrological paradigm of phase separation and shallow mixing can explain much of the geochemical and biological variation seen in Yellowstone's hydrothermal fluids, our understanding of these processes is limited to a two-dimensional perspective. We can measure a pool's surface temperature, chemical composition, and biological characteristics, but our knowledge of the aquifer source lithologies, the subsurface architecture and fluid pathways, and the timescales of the fluid movement through these pathways are unknown. Furthermore, the significance and timescales of reactive transport in controlling the chemistry of phase-separated fluids generated in continental hydrothermal systems and its influence on microbial diversity have yet to be explored. This lack of fundamental information about Yellowstone's hydrothermal processes, in turn, limits interpretations of why such a stark difference exists in the taxonomic and functional diversity of microbial communities that inhabit these spring types.

To better understand how subsurface geological processes, such as reactive transport, phase separation, and shallow groundwater mixing, support microbial ecosystems and influence patterns in microbial diversification, we examine two adjacent, high-temperature pools in Norris Geyser Basin, Yellowstone National Park- Perpetual Spouter (Fig. 1), which is an alkaline-chloride spring (pH ~7.5) and an acid-sulfate pool known informally as "Red Bubbler" (pH ~3). Using this phase-separated hydrothermal system as a natural laboratory, we combine, for the first time ever, near-surface geophysical measurements to examine the architecture, geometry, and porosity of fluid pathways; radiogenic isotopic measurements to establish the different aquifer's lithologies and the significance of gas-water-rock interaction in determining the water's distinctive chemistries; and U- and Th-decay series isotopes to determine the timescales of water-rock interaction. We then apply metagenomic sequencing and informatics analysis of microbial communities inhabiting these springs, in the context of 56 metagenomes from other hot springs, to examine the consequences of variation in these dichotomous hot spring characteristics on the composition and function of microbial communities that inhabit these springs.

This coupling of methods provides a unique understanding of the interconnectedness of physical, chemical, and biological processes within this dynamic system and, more broadly, the bimodal differentiation of hot spring processes and microbial ecosystems observed across Yellowstone and continental hydrothermal systems in general (Brock, 1971). Specifically, we show that the bimodal distribution of phase separated systems is the result of feedbacks between the geochemical and biological (taxonomic and functional) composition of hot springs. Subsurface processes drive phase separation and control reactive transport on variable timescales as inferred by isotopic measurements, and then this variation drives differences in microbial taxonomy and metabolism, which in turn additively contributes to a hydrothermal system's geochemical bimodality.

2. METHODS

2.1 Geophysical Methods

The geophysical methods employed for this discussion are 2D-DC resistivity imaging, ground penetrating radar, and surface Nuclear Magnetic Resonance (NMR) sounding. The goal of the geophysical study was to: 1) image any structural controls on existing hydrothermal pathways, 2) identify zones of active water permeability, and 3) potentially image steam or gas zones within the subsurface to understand near surface phase separation or mixing.

DC resistivity data were collected in a 2D profile line using an AGI SuperSting R8 system with 112 electrodes at 1 m spacing. These 2D resistivity data were collected with a mixed array composed of dipole-dipole and strong gradient configurations. The two pools were centered within the 2D resistivity profile. Resistivity data were processed using R2 software (Binley, 2015). Inversion parameters include: uniform starting model equal to the average of the apparent resistivity, 140 Ohm m; error model of a = 0.02, b = 0.04; convergence in three iterations to a final error-normalized RMS misfit of 1.00 and depth of investigation (DOI) values were calculated following Oldenburg and Li, 1999. The vertical ground temperature gradient was removed by correcting all resistivity values to a standard of 18°C using the approach of Keller and Frischknecht, 1966 and the interpolated temperature measurements in Y-9 borehole near the Two Pools site (White et al., 1975).

Ground penetrating radar (GPR) data were acquired using a Noggin with 250 MHz shielded antennae (Sensors & Software, Mississauga, Canada), a trace spacing of 0.03 m, a time

155	window of 60 hs and a sampling rate of 2.5 GHz. Data were processed using Reflex w
156	(Sandmeier Geophysical Research, Karlsruhe, DE) using conventional filters and corrections:
157	dewow, linear gain function, correct start-time, frequency bandpass (150 MHz $-$ 600 MHz), and
158	Kirchhoff migration ($v = 0.065 \text{ m ns}^{-1}$, determined by minimizing over/under migration
159	artifacts).
160	Surface NMR data were acquired with a GMR instrument (Vista Clara Inc., Mukilteo,
161	WA). The NMR sounding location was centered on Perpetual Spouter. The primary
162	transmitting/receiving and noise loops were deployed in a "figure 8" pattern to minimize the
163	effect of external electromagnetic noise on the measurements. The "noise compensation loop"
164	was placed NE of the primary loop. Prior to deployment of the primary loops, a proton
165	precession magnetometer was conducted to determine if any large (> 500 nT) magnetic gradients
166	were present at the site. With no large magnetic gradients detected, the NMR system was
167	deployed and acquired with 16 stacks at a local Larmor frequency (2255.6 Hz). NMR data were
168	processed and inverted using MRSMatlab software (Müller-Petke et al., 2016). Inversion
169	parameters included: regularization factor of $6x10^3$ determined by L-curve analysis; vertical
170	discretization of 1 m, sensitivity kernel built using resistivity structure determined from 2D-DC
171	Resistivity, final goodness-of-fit $X^2 = 1.1$. Further details on the geophysical methods can be
172	found in Supplementary Methods A.
173	
174	2.2. Geochemical Analytical Methods
175	Sr, Nd, Pb radiogenic isotopes (see supplement in Sims et al., 2013) and ²³⁸ U- ²³⁰ Th were
176	measured by mass spectrometric methods and ²²⁶ Ra and ²²⁸ Ra were measured by both gamma
177	counting methods and high abundance sensitivity plasma mass spectrometry (Layne and Sims,
178	2000; Sims et al., 2008a, b, 2013; Scott et al., 2019). ²²² Rn and ²²⁰ Rn were measured by in situ
179	alpha counting of ²¹⁸ Po and ²¹⁶ Po using the Durridge RAD7 (Giammanco et al., 2007; Lane-
180	Smith and Sims, 2013; Giammanco and Sims, 2022) and ²²³ Ra and ²²⁴ Ra were measured by
181	radium delayed coincidence counting (RaDeCC) measurement of Mn-fibers.
182	
183	2.2.1 Sampling and Chemical Purification of Hot Spring Fluids

Sampling and Chemical purification for Mass Spectrometry

Hydrothermal water samples from Perpetual Spouter and Red Bubbler were collected for isotopic analyses during two separate field trips (July 2014 and August 2015). Hydrothermal water was pulled into a Luer-lock syringe and filtered through 0.1 μ m to remove colloidal particles. Waters were filtered into acid washed LDPE bottles, and each sample was acidified in the field with ~1 ml 6M HCl for every 50 ml of sample water collected.

In the laboratory, filtered hydrothermal water samples were dried in preparation for chemical purifications using column chromatography modified from our laboratories well-established procedures (Layne and Sims, 2000; Thirlwall, 2002; Sims et al., 2008a, b; Scott et al., 2019). Dried samples were fluxed with concentrated HNO3 and sat overnight to fully oxidize the sample. Samples were then dried and re-dissolved in nitric acid for separation of U and Th from the bulk sample matrix using a large (10 ml column volume) anion exchange column in nitric acid. The U-Th fraction was dried and re-dissolved in 11M HCl + H₂O₂ for separation of Th from U using a smaller (1 ml column volume) anion exchange column in HCl. The separated U and Th fractions were dried in preparation for mass spectrometry.

The bulk sample matrix from the first large anion column was dried and re-dissolved in $6M \ HCl + H_2O_2$ for purification of Fe from the bulk sample matrix. The same large anion column was used to remove Fe from the remaining bulk sample matrix, however the purification uses HCl rather than HNO₃. The Fe fraction from this procedure was dried and refluxed in concentrated HNO₃ to maintain full Fe oxidation. The Fe procedure was repeated using a smaller (1 ml column volume) anion column in HCl to ensure complete Fe purification. The final Fe fraction was dried in preparation for mass spectrometry.

The remaining bulk sample matrix from the Fe chemistry was dried and redissolved in 1M HBr for purification of Pb from the bulk sample matrix. An anion column (2 ml column volume) in HBr was used, and the purified Pb fraction was dried in preparation for mass spectrometry. The remaining bulk sample matrix was collected and dried for further chemical procedures.

The bulk sample matrix containing the remaining Sr, Nd, and Ra was dissolved in 1M HCl for separation of the three remaining fractions using a cation exchange column (4 ml column volume). Sr, Nd, and Ra were each removed from the cation exchange column in separate aliquots. The Sr and Nd fractions each required one further purification on a SrSpec (0.3 ml column volume) and LnSpec (0.5 ml column volume) column, respectively. Final purification

of Ra involves a SrSpec (0.5 ml column volume) column procedure (performed twice) followed by a final anion exchange column (0.5 ml column volume) to remove ²²⁸Th that grew in during the sample processing procedures. The final Sr, Nd, and Ra fractions are all dried in preparation for isotopic and concentration analysis by mass spectrometry.

220

221

222

223

224

225

226

227

228

229

230

231

232

233

234

235

236

237

238

239

240

241

216

217

218

219

Sampling and Chemical purification for Counting Methods

The technique we have chosen for the short-lived isotopes of Ra (²²⁴Ra, ²²³Ra and ²²⁸Ra), Mn-fiber Ra extraction, is a reliable and robust method, originally developed for shipboard collection on ocean cruises that utilizes Mn-oxide impregnated acrylic fibers (Mn-fibers) to scavenge Ra from seawater (Moore and Reid, 1973; Moore, 2008). The Mn-fiber extraction technique is particularly well-suited for the measurement of Ra in continental hydrothermal fluids for the following reasons: 1) all four Ra isotopes can be accurately determined from a single Mn-fiber sample; 2) Mn-fibers quantitatively adsorb Ra (Moore and Reid, 1973; Moore, 2008) at relatively fast flow rates, up to 1 liter per minute; 3) radium delayed coincidence counting (RaDeCC) measurement of Mn-fibers is a fast and efficient method for low-activity ²²³Ra and ²²⁴Ra, which is essential for achieving the high sample throughput required for such short-lived isotopes; and, 4) Mn-fiber Ra pre-concentration techniques do not inherently require large, expensive high volume pumps and shipboard laboratories, but can be exploited as an easily portable and simple in-situ method compatible with the limitations associated with sampling remote and difficult to access continental hydrothermal features often located in rugged terrain and ecologically fragile environments (e.g. Yellowstone). Following Ra extraction, Mn-fibers are transported from the field to a laboratory (or mobile laboratory for measurement of short-lived Ra) where ²²⁴Ra and ²²³Ra activities are measured on a RaDeCC following the methods of Moore (2008). Subsequently the Mn-fibers are ashed for gamma spectrometry measurement of ²²⁸Ra and counted with a high-purity germanium well-type detector using methods detailed in Henderson et al., 2013.

242

243

244

245

246

Because of the extreme water chemistry of Yellowstone thermal fluids, which ranges in pH from acidic to basic (1.4 - 9.8), Eh (-0.231 - 0.831 V) and temperature (ambient to $93 \,^{\circ}$ C, which is boiling at Yellowstone's elevation of $\sim 2,000 \, \text{m}$) quantitative extraction of Ra on Mn fiber requires: 1) adequate sample size; 2) efficient Ra extraction and retention on Mn-fibers across a

large range of pHs; and, 3) mitigating the potential effects of particulate bound Ra associated with large variations in suspended sediment load in hot spring waters.

2.2.2 Mass Spectrometric Methods

All isotopic and solution concentration measurements were completed on the NeptunePlus multi-collector inductively coupled plasma mass spectrometer (MC-ICPMS) at the High Precision Isotope Laboratory at the University of Wyoming. Chemically separated and purified Fe aliquots were dried and then re-dissolved in 1N (5%) HNO₃ at least 2 hours prior to analysis. These Fe aliquots were diluted to match standard Fe concentrations, generally ~400 ppb, and Fe isotopes were analyzed using medium-resolution mode and an Apex desolvating nebulizer introduction system. Sample-standard bracketing was used to correct for mass bias. Each individual sample was analyzed at least three times between individual IRMM-014 standard analyses. Reported errors are two-standard deviation confidence intervals for each hydrothermal fluid sample (Sims et al., 2008a; Dutton et al., 2017).

Purified Sr and Nd were dissolved in 5% HNO₃ for isotopic analysis of the 87 Sr/ 86 Sr and 143 Nd/ 144 Nd in static mode using either an Apex or Aridus II desolvating nebulizer. All isotopes of Sr and Nd were measured in individual faraday collectors, and additional collectors were used to monitor and correct for interferences from Rb and Kr for Sr and Ce and Sm for Nd. Internal corrections for mass bias were applied assuming 86 Sr/ 88 Sr = 0.1194 and 146 Nd/ 144 Nd = 0.7219. The Sr isotopic standard NBS987 and Nd isotopic standards LaJolla and Jndi-1 were measured to assess accuracy, and final isotopic compositions are reported relative to NBS987 87 Sr/ 86 Sr = 0.71024, LaJolla 143 Nd/ 144 Nd = 0.51185, and Jndi-1 143 Nd/ 144 Nd = 0.512107.

Purified Pb aliquots were dissolved in 5% HNO₃ for isotopic analysis of 208 Pb/ 206 Pb and 207 Pb/ 206 Pb using either an Apex or Aridus II desolvating nebulizer. Thallium was added to each sample to correct for mass fractionation with Pb/Tl ratio target of \sim 3/1. Lead and thallium isotopes were analyzed in static mode using six Faraday collectors with ratios normalized to 203 Tl/ 205 Tl = 0.418922 to account for instrumental mass bias. A seventh Faraday collector was used to monitor mercury. Lead isotope ratios are reported relative to NBS981 values of Thirlwall (Thirlwall, 2002).

Purified U and Th aliquots were dissolved in 5% HNO₃ for isotopic analysis of the ²³⁰Th/²³²Th and ²³⁴U/²³⁸U ratios using an Apex desolvating nebulizer. These isotopic ratios are on

the order of 10⁻⁶ and 10⁻⁵ and require the use of combined faraday – ion counter measurements. Mass bias, ion counter yield, dark noise, and RPQ transmission were corrected for using sample standard bracketing and isotopic standards IRMM-035 for Th and U010 for U. In addition to isotopic ratios, total yields of U and Th were measured relative to ICP CertiSpex concentration standards to obtain the activities of individual nuclides in the hydrothermal fluids. Column chemistry yields for these procedures are no less than 70%; therefore, we assign a conservative error estimate for individual activities of 30%.

Purified Ra aliquots were dissolved in 5% HNO₃ for isotopic analysis of the ²²⁸Ra/²²⁶Ra ratio using an Apex desolvating nebulizer. The NeptunePlus at the University of Wyoming is equipped with a dual SEM-RPQ collector block, which was used for static measurement of both isotopes of radium (Scott et al., 2019). Mass bias, ion counter yields, and dark noise were accounted for using sample-standard bracketing and an internal ²²⁸Ra/²²⁶Ra standard, first calibrated and measured in 2009. Total Ra yields were measured relative to the NIST4967 ²²⁶Ra standard. As with U and Th, the column chemistry procedures yield no less than 70% recovery, and we assign a conservative error of 30% to the individual activities of ²²⁸Ra and ²²⁶Ra.

293

294

278

279

280

281

282

283

284

285

286

287

288

289

290

291

292

3.2.3 Ra Delayed Coincidence Counting (RaDeCC):

- 295 The short-lived Ra isotopes (224Ra and 223Ra) are measured on a radium delayed coincidence
- 296 counter (RaDeCCTM) which measures ²²⁴Ra and ²²³Ra by proxy of the alpha decays from their Rn
- daughters (²²⁰Rn and ²¹⁹Rn respectively) via a Lucas cell and attached photomultiplier tube; the
- delayed coincidence counter discriminates between Rn isotopes (see Moore and Arnold, 1996;
- 299 Moore, 2008; Moore and Cai, 2013). Each Mn-fiber sample is counted three times: 1) within 0-5
- 300 days of extraction for optimal ²²⁴Ra determination; 2) after 8-11 days to reduce uncertainty for
- 301 223 Ra associated with "chance coincidence" interference from 224 Ra; and 3) after \sim 70 days to
- determine the supported ²²⁴Ra and ²²³Ra activities (Moore, 2008).

303304

2.2.4 Gamma Spectrometry:

- 305 The longer-lived ²²⁸Ra and ²²⁶Ra are determined by ashing the Mn-fibers in a muffle furnace at
- 306 400 °C to achieve an appropriate mass and geometry for gamma spectroscopy using 25mm
- 307 polystyrene vials and a Canberra Industries Inc. high-purity germanium well-type detector. The
- vials are sealed (with a thin silicon plug and 5mm of epoxy) for ≥ 22 days to allow for Rn

daughter ingrowth. ²²⁸Ra activity is calculated from 338 and 911 keV (from ²¹²Pb and ²²⁸Ac 309 respectively) peaks and ²²⁶Ra is determined from 295, 352, and 609 keV peaks (from ²¹⁴Pb, 310 ²¹⁴Pb, and ²¹⁴Bi respectively). 311 312 313 2.3 Molecular Methods 314 2.3.1 Sample Collection and DNA extraction. 315 Samples for molecular characterization of planktonic and sediment-associated communities were 316 collected on May 22, 2017, as previously described (Fernandes-Martins et al., 2023). Duplicate 317 sediment samples were collected from each spring using a sterilized spatula and placed in sterile 318 2.0 mL cryotubes. Duplicate samples of filtered water were collected using a peristaltic pump 319 from a depth of ~20 cm beneath the spring surface. An aluminum in-line filter housing 320 containing a 47 mm diameter, 0.22 µM pore-size Supor filter (Pall, Port Washington, NY) 321 connected to Teflon tubing was used to collect planktonic cells. Prior to placing the sterile filter 322 in the housing, ~2 liters of spring water were pumped through the housing and the tubing to 323 minimize introduction of non-endogenous cells and their genomic DNA. The filter was then placed in the housing using ethanol-sterilized forceps and 6 liters of water was passed through 324 325 each filter. Filters containing biomass were placed in sterile 50 mL tubes and were immediately 326 frozen on dry ice. Sediments and filters were stored at ~80°C until further processing. A Fast 327 DNA Spin Kit for Soil (MP Biomedicals, Irvine, CA) was used to extract genomic DNA from 328 each sample following the manufacturer's protocols. DNA extracts were quantified using the 329 Qubit DNA HS Assay kit and a Qubit fluorometer (Molecular Probes, Life Technologies, 330 Madison, WI) and frozen at -20°C until further processing. 331 332 2.3.2 Metagenomic Sequencing, Assembly, and Genomic Reconstruction. 333 DNA extracts were subjected to shotgun metagenomic sequencing at the Department of Energy 334 Joint Genome Institute (JGI; Walnut Creek, CA) following standard library preparation 335 protocols. Sequencing was conducted on the Illumina Novaseq platform with paired-end 2 x 150 336 bp sequencing. Reads were quality-filtered, trimmed, and cleaved of Illumina-specific 337 sequencing adapters using BBTools (sourceforge.net/projects/bbmap/) and then read corrected 338 using bfc (v.r181) (Li, 2015) via the standard JGI metagenome processing pipeline. Reads were 339 then assembled into contigs using SPAdes v.3.13.0 (Nurk et al., 2013) with the following

specifications: -m 2000 --only-assembler --meta. Metagenome-assembled-genomes (MAGs) were constructed from the assembly, as previously described (Colman et al., 2022). Briefly, the metaWRAP pipeline (v.1.3.2) (Uritskiy et al., 2018) was used to map paired-end reads to the assembled contigs using the BWA aligner and MAGs were generated from assembled contigs (specifying an -1 of 2500) based on similarities in sequencing depth coverage profiles and tetranucleotide frequency usage with the MetaBAT v.2 (Kang et al., 2015), MaxBIN v.2 (Wu et al., 2014), and CONCOCT v.1.1.0 (Alneberg et al., 2014) genome binning algorithms. The bin refinement module of metaWRAP was used to select the highest quality MAG dataset for each metagenome from the various binning strategies and by assessing contamination and completeness estimates of MAGs using CheckM v.1.0.5 (Parks et al., 2015). Only medium-high quality draft MAGs (>50% completeness, < 10% contamination) were included in the final analyses. Gene prediction and annotation was conducted using prokka v.1.13 (Seemann, 2014). Relative abundances were calculated for individual populations with the 'profile' function within CheckM wherein relativized abundances are first calculated from the mapping of reads to individual MAGs and then normalized to estimated MAG sizes. Finally, relative abundances were normalized to all estimated abundances within communities. Whole-metagenome sequence diversity was calculated using a genome bin-independent approach via the Nonpareil (v.3.304) metric and the quality-filtered reads for each metagenome. Briefly, sequence diversity and coverage estimates are derived from Nonpareil sequencing coverage curves and evaluate the level of sequence redundancy within a metagenomic dataset to then approximate the extent of expected diversity that is covered by the actual sequencing effort (Rodriguez-R et al., 2018).

361362

363

364

365

366

367

368

369

370

340

341

342

343

344

345

346

347

348

349

350

351

352

353

354

355

356

357

358

359

360

2.3.3 Metagenome Analyses and Metabolic Inferences.

To compare the functional proteins encoded in each MAG, the KEGG Orthology (KO) assignments for each assembled metagenome were collected by comparison against the KEGG automatic annotation server (KAAS) (Moriya et al., 2007). The KO data were used to construct a presence/absence table for each MAG via adaptation of a MATLAB script (https://github.com/dcolman1/). Of the entire KO dataset, only those database annotations associated within the KEGG 'Energy Metabolism' category were used in further analyses to include only data that were most pertinent in discerning the relationship between spring

geochemistry and microbial metabolism. A Jaccard dissimilarity matrix was constructed from the normalized dataset using the 'vegdist' function within the vegan package (v.2.4-4) for R and the distance matrix was subjected to principal coordinates analysis ordination in R (Oksanen et al., 2022; https://cran.r-project.org/web/packages/vegan/). In addition, a matrix describing the similarity in KEGG profiles of Red Bubbler and Perpetual Spouter were included within a larger analysis of 54 other chemosynthetic Yellowstone metagenomes that are components of our other ongoing studies. Briefly, KEGG assignments were collected from the Integrated Microbial Genomes (IMG) or KAAS platform for metagenomes and used to build a compositional matrix as described above, but weighted by the instances a KO was identified in a metagenome and only including KO annotations involved in the 'Energy Metabolism' category. The fraction of proteins annotated to the 'Sulfur Metabolism' category among all of the 'Energy Metabolism' annotated proteins was evaluated to assess whether Red Bubbler and Perpetual Spouter populations exhibited trends in "Sulfur Metabolism" consistent with those previously documented for chemosynthetic Yellowstone springs (Payne et al., 2019).

In addition to KEGG assignments for some protein ortholog groups, BLAST-based searches were conducted against the annotations for all MAGs. Specifically, MAGs were queried via BLASTp for specific gene functions, guided by gene contents in closely related genomes to screen for specified metabolic functions using bait sequences specific for the active site subunits for each of the proteins or protein complexes. Positive matches within MAGs were considered as those with an E-value > 1x10⁻⁶, >30% amino acid homology, and >60% of the length of the BLASTp bait sequence. The assembled metagenome data for the Perpetual Spouter samples are available in IMG under accessions 3300033484 (plankton) and 3300033491 (sediment) and those for the Red Bubbler samples are available in IMG under accessions 3300033476 (plankton) and 3300033830 (sediment).

3. RESULTS

All data are presented in Tables 1-3, Figures 1-7 and in the *Supplemental Tables S1-S5*. Major and trace element chemistry are from (McCleskey et al., 2014; 2022b) and presented in *Supplemental Materials, Table S1*. *Supplemental Materials, Table S5* provides isotopic measurements of USGS standard reference materials compared with literature values as a measure of quality assurance.

3.1 Two Pools: A Natural Laboratory to Examine Phase Separation

Phase separation results from decompression boiling and is thus a continuous process that occurs over a multitude of scales. However, for our study we focus on two adjacent phase separated pools Perpetual Spouter and Red Bubbler.

These "Two Pools", Perpetual Spouter and Red Bubbler, represent an ideal natural laboratory to investigate phase separation processes: 1) their surficial separation of 14 meters provides optimal scaling resolution for the geophysical measurements; 2) their subsurface geology is well constrained from three nearby boreholes (White et al., 1975); and 3) they have characteristic bimodal chemistries (Fig. 1).

The Two Pools site is in the Norris Geyser Basin (NGB), which is at the intersection of the Norris-Mammoth Corridor structural complex and the eastward extension of the Hebgen Lake fault system (Fig. 1a). Albeit outside the northwest rim of the Yellowstone caldera, NGB is one of Yellowstone's major hydrothermal basins and arguably one of its most active and spectacular. NGB has Yellowstone's highest measured surface and subsurface temperatures (Allen and Day, 1935; White et al., 1975), contains a great diversity of physical features (geysers, mud pots, etc.) and chemical variability, and is one of Yellowstone's most dynamic geyser basins, experiencing considerable uplift and subsidence (Chang et al., 2007, 2010). The minimum heat flow across the Norris Geyser Basin is 300-340 W/m² with the hydrothermal subbasin hosting Perpetual Spouter and Red Bubbler having an average minimum heat flow of ~310 W/m² (Heasler and Jaworowski, 2018). Maximum heat flow measurements for Norris Geyser Basin are variable, dependent on the existence and concentration of hydrothermal features at the surface. NGB also experiences significant periodic hydrothermal disturbances, during which the chemistry, activity, and nature of hydrothermal features in NGB can change drastically over

short timescales (weeks to years) (White et al., 1975, 1988; Fournier et al., 2002; Colman et al., 2021). These hydrothermal disturbances are linked to changing interactions between the deep hydrothermal system and the surrounding shallow groundwater system (Fournier et al., 2002), the latter of which is more susceptible to recharge through recent precipitation (Colman et al., 2021). However, the nature and magnitude of the changes in these interactions are not well understood (Fournier et al., 2002).

Three boreholes (i.e., C-II, Y-9, Y-12) have been drilled in NGB (Allen and Day, 1935; White et al., 1975; Jaworowski et al., 2016) to investigate a region in the Yellowstone system dominated by acidic waters (Hole C-II) (Allen and Day, 1935) and high heat flow. Y-9 is the closest borehole to the Two Pools site. Except for Y-9, which starts in a thin surface layer of silica sinter and sinter-cemented glacial gravel and till (down to ~1 meter), Lava Creek Tuff (LCT) is the only lithology present in all three holes (maximum drilling depth of 331.6 meters at Y-12 (White et al., 1975)). Both LCT members, "A" (lower unit) and "B" (upper unit), are present in these boreholes, with the contact between these two units located from 23.8 meters (C-II) to 38.9 meters (Y-9) (White et al., 1975, 1988). C-II is an endmember amongst these holes and as such it is the most representative of a shallow vapor-dominated system and its concomitant hydrothermal alteration (White et al., 1975). Although none of the boreholes penetrated beyond the LCT, the regional geology suggests that a thick sedimentary package of Paleozoic and Mesozoic sandstones, shales and carbonates underlie the LCT in this region (Anon, 1972). For further information on the cores and the downhole measurements, such as change in temperature with depth, which does not follow model geotherms, the reader is referred to (Allen and Day, 1935, White et al., 1975, 1988).

Perpetual Spouter and Red Bubbler are located at the base of Ragged Hills along Tantalus Creek, downstream from the Back Basin of NGB (Fig. 1b). Ragged Hills, which form an elevated south-western margin of NGB, are thermal kames of ice-contact sediments, up to 30 meters thick (Richmond and Waldrop, 1975; White et al., 1988; Fournier et al., 2002; Jaworowski et al., 2006). These thermal kames formed at the end of the Pinedale glaciation (22-13 ka) when melting ice deposited sand and gravel within an active hydrothermal area, leaving behind thick clastic deposits that were indurated and cemented by opal and retain a fairly high porosity on a variety of length scales (Richmond and Waldrop, 1975; White et al.,

1975, 1988; Fournier et al., 2002; Jaworowski et al., 2006, 2016). The surface of the Two Pools site is hard and rocky with each spring emerging from distinct pools. Both are precipitating mineral deposits: Perpetual Spouter is depositing silica sinter, Red Bubbler is depositing alternating layers of hematite and silica – much like banded iron formations.

Perpetual Spouter, named by Hague and others in 1904 (Hague, 1904), is an alkalinechloride pool with a temperature of ~90°C, a pH of ~7.5, low SO₄²-(~37 mg/L) and high Cl⁻ (~790 mg/L) (Supplemental Materials, Table S1). The conduit of Perpetual Spouter is lined with silica sinter precipitate to an unknown depth. This silica sinter lining greatly limits shallow water-rock interaction between Perpetual Spouter's waters and the underlying LCT. Na/K geothermometry estimates the Perpetual Spouter reservoir at about 210 °C using the Truesdell equation and at about 250 °C using either the Fournier or the Giggenbach equation (Tuesdell and Fournier, 1976). Because silica is being precipitated during upflow, the preferred temperature is 250 °C (White et al., 1992). Despite periodic thermal disturbances in other systems in NGB, Perpetual Spouter's geochemical composition has remained remarkably constant over both long and short timescales (Fournier et al., 2002). Measurements of tritium show that Perpetual Spouter's waters (measured from 1967-1976) are best modeled as a mixture of 7% tritiated water with a short residence time (10 years), and thus presumed to be shallow recharge, and 93% tritium-free waters which are hypothesized to be from a deep reservoir (Pearson and Truesdell, 1978; Gardner et al., 2011). Perpetual Spouter's flow rate appeared to be consistent over the time of measurement.

Red Bubbler is an acidic, ephemeral pool with a temperature of ~88°C, a pH of ~3, high SO₄²⁻ (~207 mg/L) and moderate Cl⁻ (~340 mg/L) (*Supplemental Materials, Table S1*) (McCleskey et al., 2014; 2022b). This relatively high Cl⁻ concentration for an acid-sulfate system requires some remixing with boiled Cl⁻-enriched waters, with the most likely candidate being water from the Perpetual Spouter system. While Red Bubbler's chemistry has remained fairly consistent, its water level exhibits considerable variability from overflowing to non-existent, to filling and refilling with regular periodicity, over a variety of timescales (hours to seasonally). In addition to Red Bubbler, there are other nearby acid-sulfate springs emanating within Tantalus Creek, and nearby high-temperature fumaroles upgradient on the flank of Ragged Hills indicating that Red Bubbler, albeit the dominant feature, is just part of a complex

and highly dynamic vapor-dominated system that is being influenced by shallow groundwater recharge.

Not surprisingly, the Two Pool's distinct chemistries result in contrasting concentrations of solutes. The dissolved ion concentrations of elements such as Pb, Fe, Nd, Sr, U, Th, and Ra in the acidic Red Bubbler waters are much higher than in waters from Perpetual Spouter, often by an order of magnitude or more, whereas elements such as Ca, Na, Cl, F, Li, B, Br, Cs, and As are all higher in Perpetual Spouter.

496

497

498

499

500

501

502

503

504

505

506

507

508

509

510

511

512

489

490

491

492

493

494

495

3.2 Near-Surface Geophysical Imaging Beneath Two Pools

GPR imaging (Fig. 2a) revealed convex up, subparallel, moderately continuous reflections which attenuate at <2 m depth that we interpret to be silica-cemented, clastic kame deposits associated with the Ragged Hills, localized Fe deposits associated with Red Bubbler, and silica sinter associated with Perpetual Spouter. The 2D-DC resistivity results show shallow prominent, but discontinuous, regions of high resistivity down to ~4 m that can be interpreted as regions of either: 1) lower bulk porosity than the surrounding material or 2) increased gas content within a laterally consistent bulk porosity. Knowledge of the surface geology and nearsurface geology from boreholes (White et al., 1975) leads us to interpret these high resistivity zones as areas with lower bulk porosity, likely regions of silica sinter and sinter-cemented clastic glacial kame deposits. Directly below Perpetual Spouter (Fig. 2b) is a narrow, vertically oriented, low resistivity zone (~80 Ohm m) that is interpreted to represent the primary conduit feeding the spring from a reservoir >10 m below the surface. Likewise, immediately below Red Bubbler, in the top 2 m, is a low resistivity zone (~30 Ohm m) that extends southwest towards Ragged Hills, (Fig. 2b) parallel to the ground surface. The surface NMR data (Fig. 2c-f) show a decrease in water content with depth that, assuming saturation, would indicate a decrease in porosity and/or a decrease in the extent of weathering.

513514

515

3.2 Isotopic Measurements

- The isotopic measurements are tabulated in Tables 1-3 and shown in Figures 3-5. Radiogenic
- Nd, Sr, Pb and Fe isotopic compositions and U- and Th-decay series abundances of Red Bubbler

and Perpetual Spouter and other relevant acidic and neutral chloride hot springs are tabulated in Tables 1 and 2. Measurements of nearby and regional volcanic and sedimentary rocks from potential aquifers for these waters are tabulated in Table 3; these data come from measurements made at the UW High Precision Laboratory and published data from other studies (Leeman et al., 1977; Doe et al., 1982; Hildreth et al., 1991; Hildreth et al., 1984; Sturchio et al., 1993).

3.2.1 Radiogenic and Stable Isotopic Measurements

The isotopic compositions of Perpetual Spouter and Red Bubbler are starkly different, particularly with regards to ²⁰⁸Pb/²⁰⁶Pb (Fig. 3a; Table 1). Red Bubbler's acid-sulfate waters exhibit a ²⁰⁸Pb/²⁰⁶Pb signal that is essentially identical to that of the Lava Creek Tuff, whereas Perpetual Spouter's alkaline-chloride waters present a substantially lower ²⁰⁸Pb/²⁰⁶Pb that is similar in value, but not identical, to that of the Paleozoic and Mesozoic sedimentary rocks buried beneath the Lava Creek Tuff in the NGB.

In contrast to ²⁰⁸Pb/²⁰⁶Pb, the ⁸⁷Sr/⁸⁶Sr of volcanic and sedimentary rocks show considerable overlap and are by themselves less sensitive for distinguishing the source characteristics of Yellowstone's hydrothermal waters. Because of low analyte concentrations for the amount of water collected (150 ml), the ¹⁴³Nd/¹⁴⁴Nd isotope measurements for Perpetual Spouter are unreliable and thus not reported. Nonetheless, and importantly, ⁸⁷Sr/⁸⁶Sr and ¹⁴³Nd/¹⁴⁴Nd of Red Bubbler's acidic waters are identical to those of Lava Creek Tuff (Tables 1&3). Finally, we note that consistency in Pb and Sr isotopic compositions measured in Perpetual Spouter and Red Bubbler over the two-year time period suggests these two pools were compositionally in a steady-state.

To confirm these isotopic differences, we extended our Sr and Pb radiogenic isotopic study to several other springs within Yellowstone National Park (Fig. 3). The extended suite includes: nearby acid-sulfate waters also hosted in LCT; the alkaline-chloride feature Beryl Spring, which is believed to represent the quintessential deep hydrothermal water beneath Yellowstone (Nordstrom et al., 2004), and is also hosted in the LCT; and, finally, waters from Mammoth Terraces and Boiling River, whose unique calcium-bicarbonate-sulfate compositions require them to have interacted extensively with the deeper Mesozoic and Paleozoic rocks (Kharaka et al., 1991; Fouke et al., 2000). The acid-sulfate samples have high $^{208}\text{Pb}/^{206}\text{Pb}$,

whereas the alkaline-chloride waters of Beryl Spring and calcium-bicarbonate-sulfate waters from Mammoth Terraces and Boiling River have low ²⁰⁸Pb/²⁰⁶Pb. We note that ²⁰⁸Pb/²⁰⁶Pb measurements from the drill core of Y-10 at Mammoth Terraces (Leeman et al., 1977) yield identical values as our measurements of calcium-bicarbonate-sulfate waters from Mammoth Terraces and Boiling River.

We also measured stable Fe isotopes in Red Bubbler and Perpetual Spouter waters and in both the LCT and the Madison Limestone (Tables 3). Our measurements for Perpetual Spouter were effectively below detection limit. For Red Bubbler δ^{56} Fe/ 54 Fe and δ^{57} Fe/ 54 Fe are identical to LCT, within uncertainty, indicating that chemical weathering in this acidic system is mobilizing Fe without isotopic fractionation.

3.2.2 U- and Th-decay series measurements

We use measurements of ²²⁸Ra and ²²⁶Ra to determine the timescales of water-rock interaction, and measurements of both long-lived (²³⁸U, ²³²Th and ²³⁰Th), and short-lived (²²⁴Ra, ²²³Ra and ²²²Rn) isotopes to constrain model parameters and to validate assumptions implicit to the application of the (²²⁸Ra/²²⁶Ra) chronometer (Fig. 4 & 5; Table 2 & 3). All nuclide abundances and ratios are given in activities, denoted by parentheses (e.g., (²²⁸Ra/²²⁶Ra)), to provide comparable units within a decay chain.

Activity ratios of (228 Ra/ 226 Ra) in Perpetual Spouter and Red Bubbler waters are drastically different from each other. Perpetual Spouter's alkaline-chloride waters have a much lower (228 Ra/ 226 Ra) of 5.9 ± 3.1 (n = 3); Red Bubbler's acid-sulfate waters have a very high (228 Ra/ 226 Ra) of 45.0 ± 6.4 (n = 3). With the exception of 222 Rn (which we suspect, as discussed in detail below, is degassing over the whole Two Pools region), the activities of the individual nuclide abundances are consistently higher in Red Bubbler than they are in Perpetual Spouter. These differences vary amongst different nuclides according to their solubilities and half-lives and thereby provide information about assumptions (e.g., the solubility of Th) and critical model parameters, such as recoil rates.

As possible rock source lithologies for our reactive transport modeling, we also provide a compilation (Table 3) of values for [U], [Th], and (²³²Th/²³⁸U) for unaltered LCT (Doe et al.,

1982; Hildreth et al., 1984, 1991) and altered LCT (as represented in Y-12 drill core from NGB (Sturchio et al., 1993)), as well as several different possible local sedimentary rock lithologies. Because of a lack of knowledge of the actual sedimentary rock(s) involved, we calculated an average Paleozoic-Mesozoic sedimentary rock composite for modeling purposes using the average [U], [Th] and (²³²Th/²³⁸U) values from Sturchio et al., 1993.

3.3 Microbial Taxonomic and Functional Biodiversity.

576

577

578

579

580

581

582

583

584

585

586

587

588

589

590

591

592

593

594

595

596

597

598

599

600

601

602

603

604

605

A total of 4 - 5 x 10⁸ sequence reads were generated from Perpetual Spouter and Red Bubbler water and sediment microbial communities. Estimation of genomic diversity coverage based on read sequence redundancy revealed exceptionally high genomic coverage (99.6%, 99.9%, 99.9% and 99.9% for the four metagenomes, respectively), suggesting that additional sequencing effort would not recover substantial additional genomic (and thus, taxonomic) diversity, unlike what is typically observed for metagenomic analyses of other microbial environments (Rodriguez-R et al., 2018). Assembly of the reads and genome-based binning from the metagenomes generated 48 genome bins (i.e., metagenome-assembled-genomes; MAGS), including 15 and 20 from Perpetual Spouter water and sediment communities, respectively, in addition to four and eight from Red Bubbler water and sediment communities, respectively (Supplemental Materials, Table S3). Of the entire metagenomic read datasets, 61.7%, 76.7%, 87.3%, and 68.8% of reads were mapped to the MAGs, respectively, suggesting a high level of fidelity between the MAG dataset to the overall metagenomic read dataset. Consequently, the MAG-based representation of the communities is reflective of the expected diversity in the systems given the high level of sequencing effort for relatively non-diverse communities, nearly 100% recovery of estimated genomic diversity, and a high degree of the read datasets mapped to the reconstructed MAGs. Ordination of a matrix describing the dissimilarity in protein homologs involved in energy metabolism that are encoded in these 48 MAGs reveals two highly resolved groups that largely correspond to each spring (Fig. 6a). The planktonic and sediment MAGs from Red Bubbler form a tight group, while the planktonic and sediment communities from Perpetual Spouter are more functionally distinct from each other, with many Perpetual Spouter sediment MAGs clustering with those from Red Bubbler sediments and water (Fig. 6a). Consistent with previous observations that an enrichment of genes encoding proteins involved in dissimilatory sulfur metabolism is a distinguishing feature of communities inhabiting acidic Yellowstone

springs relative to those in circumneutral/alkaline springs (Colman et al., 2019; Payne et al., 2019), the Red Bubbler communities were substantially enriched in proteins involved in dissimilatory sulfur metabolism whereas the Perpetual Spouter communities were less enriched (Fig. 7). Communities from both springs clustered among other springs with similar pH, when considering 54 other metagenomes from 46 springs spanning much of the geochemical diversity of Yellowstone (Fig. 7; *Supplemental Materials, Table S2*). Thus, the communities of the two pools were representative of the variation in community composition that is observed across the broader Yellowstone geothermal system.

606

607

608

609

610

611

612

613

614

615

616

617

618

619

620

621

622

623

624

625

626

627

628

629

630

631

632

633

634

635

To further assess putative taxonomic and functional differences among communities, MAGs were subjected to metabolic reconstructions from which their putative functions were predicted (Figs. 6b & 6c; Supplemental Materials Table S4). Despite similar functional profiles of the Red Bubbler planktonic and sediment communities (Fig. 6a), they have highly different taxonomic compositions. Both communities are dominated by Archaea primarily within the Sulfolobales class, albeit different Sulfolobales taxa dominated the water and sediment communities (Fig. 6b). Specifically, the planktonic community was almost completely dominated (>99% of the community) by an uncultured Sulfolobales 'Acd1' population that represented < 5% of the sediment community. The sediment community was taxonomically more evenly distributed and comprised MAGs closely related to characterized aerobic Sulfolobaceae-like Sulfurisphaera (i.e., the QEFN01 group), Saccharolobus, and Acidianus, in addition to the anaerobes Acidilobus, Vulcanisaeta, and Thermoproteus (Supplemental Materials, Table S3). Despite taxonomic differences, MAGs comprising both the planktonic and sediment communities in Red Bubbler encoded similar suites of proteins that are involved in the dissimilatory reduction or oxidation of various sulfur compounds that include hydrogen sulfide (H₂S), thiosulfate (S₂O₃²-), and native sulfur (S⁰) (Fig. 6b; Supplemental Materials, Table S4). Sediment MAGs, including that for the most dominant sediment Sulfolobales population, also encode homologs of sulfocyanin enzymes that allow for aerobic oxidation of ferrous iron (Fig. 6b; Supplemental Materials, Table S4). The capacity for either arsenite (As(III)) oxidation or arsenate (As(V)) reduction, in addition to the reduction of oxidized nitrogen compounds (e.g., nitrate, NO₃⁻; nitrite, NO₂⁻, or nitrous oxide, N₂O) were not observed in any of the Red Bubbler MAGs (Fig. 6b; Supplemental Materials Table S4).

In contrast to Red Bubbler populations, the dominant populations represented by MAGs in the Perpetual Spouter planktonic and sediment communities are taxonomically similar and comprise both archaeal and bacterial populations (Fig. 6c; Supplemental Materials, Table S3). The dominant MAGs in both plankton and sediment communities (~42 and 72% of communities, respectively) are closely related to an uncultivated taxon affiliated with the Caldarchaeales group (formerly 'Aigarchaeota'). Metabolic reconstruction suggests these Archaea to be aerobic and facultatively autotrophic. The Perpetual Spouter Caldarchaeales MAGs encode several homologs of enzymes needed for the 3-hydroxypropionate/4-hydroxybutyrate pathway of CO₂ fixation and homologs of enzymes putatively enabling the reduction of As(V), in addition to the oxidation of H₂S and carbon monoxide (Fig. 6c, Supplemental Materials, Table S4). The putative ability of populations to reduce As(V) was also indicated among many other Perpetual Spouter MAGs that were primarily recovered from sediment communities. Moreover, populations with the potential ability to oxidize As(III) were also present in the water and sediment communities of Perpetual Spouter, namely an abundant *Thermocrinis* MAG. The potential ability to reduce oxidized nitrogen compounds (e.g., NO₃-, NO₂-, or N₂O) was also prevalent among MAGs in both the sediment and planktonic communities of Perpetual Spouter. The capacity for Fe(II) oxidation was implicated in some Perpetual Spouter populations, but only those in very low abundance (< \sim 1%) of the total community.

654

655

656

657

658

659

660

661

662

663

664

636

637

638

639

640

641

642

643

644

645

646

647

648

649

650

651

652

653

4. DISCUSSION:

In this contribution, we examine two adjacent, high-temperature pools in Norris Geyser Basin, Yellowstone National Park- Perpetual Spouter (Fig 1), which is an alkaline-chloride spring (pH ~7.5) and an acid-sulfate pool known informally as Red Bubbler (pH ~3). We combine, for the first time ever, near-surface geophysical measurements to examine the architecture, geometry, and porosity of fluid pathways; radiogenic isotopic measurements to establish the different aquifer's lithologies and the significance of gas-water-rock interaction in determining the water's distinctive chemistries; and U- and Th-decay series isotopes to determine the timescales of water-rock interaction. We then apply metagenomic sequencing and informatics analysis of microbial communities inhabiting these springs to examine the

consequences of variation in these dichotomous hot spring characteristics on the composition and function of microbial communities that inhabit these springs. This coupling of methods provides a novel understanding of the interconnectedness of physical, chemical, and biological processes within this dynamic system and more broadly, the bimodal differentiation of hot spring processes and microbial ecosystems observed across Yellowstone and elsewhere.

4.2 Subsurface Architecture Beneath Two Pools: Evidence of shallow recharge and waterrock interaction

Our geophysical imaging provides unique information on subsurface architecture critical to understanding fluid movement in Yellowstone hydrothermal systems (Pasquet et al., 2016; Bouligand et al., 2019; Smeltz et al., 2022; Ciraula et al., 2023b, a) and more specifically in this Two Pools system. Given the decrease in porosity (Fig. 2c) and relaxation time (i.e., decrease in fracture aperture/pore size, Fig. 2d) with depth observed by surface NMR, and the general decrease in resistivity with depth observed with 2D-DC resistivity, we conclude that the deeper water is very solute-rich, exists in small pores or fresh fractures, and that there is some mixing with meteoric water towards the surface in larger pores or weathered fractures. This is evidence of an overall decrease of LCT alteration with increasing depth and is consistent with visual and petrological investigations of borehole Y-9 (White et al., 1975).

The surface NMR data (Fig. 2c, d) allow us to make general interpretations about the specific surface area of the formation as a function of depth. While we cannot quantitatively interpret flow from surface NMR measurements, co-interpretation of the porosity and relaxation time (a proxy for surface area to volume ratio) is known to be a qualitative indicator of permeability as a formation flow property (e.g., Walsh, 2008). From the ground surface to ~8-m-deep, the substrate has high water content/porosity (~0.15 m³/m³) and relatively long T_2 * (~0.32 s), indicative of a porous matrix substrate. From ~8 m to ~18 m below the surface, there is a decrease in water content/porosity (~0.1 m³/m³) and a corresponding decrease in T_2 * (~0.06 s) that would be consistent with a granular matrix material with smaller pores; i.e., less weathering than the material between 0-8 m, assuming identical parent material. Finally, below 18 m, we observe a further decrease in porosity (~0.05 m³/m³) and a corresponding increase in T_2 * (>0.1 s) that are consistent with fractured material that has low water content, but relatively high bulk porosity due to open fracture apertures that are larger than the pores of granular

material. This has implications for reactive transport because the transition from highly weathered porous material to a substrate that is more closely related to fractured rock is likely to also correspond to a change from lower permeability and higher surface area (slower flow/transport, higher geochemical reactivity) to higher permeability and lower surface area (faster flow/transport, lower geochemical reactivity). While the 1D surface NMR dataset only allows us to consider this in a general sense due to the lack of spatial information, the 2D Electrical Resistivity Tomography (ERT) image (Fig. 2b) adds the extra dimension that allows the interpretation that heterogeneous development of porous, permeable substrate in the subsurface leads to areas of low permeability/low weathering (i.e., >10³ ohm m, Fig. 2b) between zones of higher permeability/higher weathering (i.e., <10³ ohm m, Fig. 2b).

While near surface geophysical imaging does not explicitly reveal direct evidence for phase separation occurring above the depth of investigation (Fig. 2), our results provide critical information necessary for understanding the subsurface architecture beneath the Two Pools. Our near surface geophysical imaging shows: 1) distinct pathways for different fluids beneath each of the Two Pools, and 2) shallow subsurface flow paths coming down from the Ragged Hills. Importantly, this shallow water recharge helps to establish the distinct chemistry of these Two Pools. When the shallow oxidized water mixes with the dispersed vapor it too helps to oxidize and acidify RB's water. And as we discuss in detail below, it is this oxidative process that facilitates reactive transport and ultimately leads to the assembly of taxonomically and functionally divergent thermophilic microbial communities.

4.3 Two Pools, Two Sources: Radiogenic Isotopic evidence for both deep and shallow gaswater-rock interaction

Albeit close together (~14 meters), and likely connected at some level below this study's geophysical depth of investigation, Perpetual Spouter and Red Bubbler have starkly different ²⁰⁸Pb/²⁰⁶Pb. These data imply that hydrothermal waters below the Norris Geyser Basin originate from a deep aquifer hosted in sedimentary rocks and that after phase separation, reactive transport processes completely shift the geochemical and isotopic compositions of Red Bubbler's waters.

Red Bubbler's ²⁰⁸Pb/²⁰⁶Pb, which is akin to the LCT, exemplifies the significant influence of shallow reactive transport. The low resistivity zone identified by the geophysical imaging immediately beneath Red Bubbler and extending southwest towards Ragged Hills is interpreted as weathered LCT that acts as a lateral conduit for meteoric water moving from the Ragged Hills to Red Bubbler. We suggest that transport through this weathered unit enables mixing of oxidized meteoric water with steam and trace H₂S vapor, and its derivatives (S⁰ and sulfide minerals), ascending from below Red Bubbler. The fluid is then oxidized in the near-surface to generate sulfuric acid ($H_2S + 2O_2 => SO_4^{2-} + 2H^+$), a process that is mediated, at least in part, by lithoautotrophic microorganisms (Mosser et al., 1973; Nordstrom et al., 2005, 2009; Colman et al., 2018) and is consistent with the observed ephemeral behavior of Red Bubbler and the enrichment of populations with the ability to aerobically catalyze H₂S/S⁰ oxidation (Fig. 6b). The acidity, in turn, promotes weathering of host rock, including leaching of acid-soluble elements (e.g., Pb, U, Fe, etc.) that then leads to high metal solute concentrations. In this case, the acidity of Red Bubbler's waters have leached enough Pb out of the LCT to completely overprint the ²⁰⁸Pb/²⁰⁶Pb of the Red Bubbler waters (Fig. 3b, Tables 1 and 3) that would otherwise be expected to be similar to Perpetual Spouter based on Cl⁻ measurements. In other words, both springs are sourced by fluids from the deep hydrothermal reservoir, but the acidity that develops in Red Bubbler, driven by oxidants available in infiltrating surface-derived fluid, leads to leaching of elements that overprints the original isotopic signatures from the deep hydrothermal reservoir. The isotopic compositions $^{87}\mathrm{Sr}/^{86}\mathrm{Sr}$ and $^{143}\mathrm{Nd}/^{144}\mathrm{Nd}$ of Red Bubbler's acidic waters are also akin to the values measured in LCT, however, it is Red Bubbler's high ²⁰⁸Pb/²⁰⁶Pb that uniquely provides conclusive evidence of shallow water-rock interaction between Red Bubbler's waters and LCT.

725

726

727

728

729

730

731

732

733

734

735

736

737

738

739

740

741

742

743

744

745

746

747

748

749

750

751

752

753

754

In stark contrast, Perpetual Spouter's alkaline-chloride waters have substantially lower ²⁰⁸Pb/²⁰⁶Pb (Fig. 3), are much less acidic, and its conduit is lined with silica sinter (>1 meter and likely deeper), armoring against shallow water-rock interactions. The low ²⁰⁸Pb/²⁰⁶Pb values in Perpetual Spouter's waters are most similar to the stratigraphically deeper Paleozoic and Mesozoic sedimentary rocks that underlie the LCT in NGB (Fig. 3b). That Perpetual Spouter's waters are not identical to the ²⁰⁸Pb/²⁰⁶Pb of the sedimentary rock lithologies suggests either shallow mixing with water that has undergone water-rock interaction with LCT, or the influence

of dissolved, locally derived dust (n.b. all samples are filtered to 0.1 microns when sampling). The very low Pb concentrations in waters from Perpetual Spouter (lower than Red Bubbler by more than an order of magnitude) make either option a possibility. However, we note that tritium measurements in waters from Perpetual Spouter point to small amounts (~7%) of shallow admixing with young, tritiated water (Pearson and Truesdell, 1978; Gardner et al., 2011). Therefore, the low ²⁰⁸Pb/²⁰⁶Pb for Perpetual Spouter strongly suggests that the alkaline-chloride waters acquired a strong component of their Pb isotopic signal from water-rock interaction with deep sedimentary rock lithologies.

These conclusions are substantiated by our supplemental measurements of ⁸⁷Sr/⁸⁶Sr and ²⁰⁸Pb/²⁰⁶Pb in nearby, hydrothermal springs. The acid-sulfate springs, which are hosted in LCT, again have ²⁰⁸Pb/²⁰⁶Pb similar to LCT, consistent with significant shallow water-rock interaction. Additionally, the alkaline-chloride Beryl Spring, considered to be an archetypical representation of the deep hydrothermal water, and the calcium-bicarbonate-sulfate waters in Mammoth Terraces and Boiling River, which have interacted extensively with limestones and anhydrites of the Mississippian Madison group (Kharaka et al., 1991; Fouke et al., 2000), have low ²⁰⁸Pb/²⁰⁶Pb, similar to the measured ²⁰⁸Pb/²⁰⁶Pb values for Paleozoic and Mesozoic limestones and sediments.

²⁰⁸Pb/²⁰⁶Pb is an important and diagnostic time-integrated radiogenic tracer of a rock's ²³²Th/²³⁸U ratio (Sims and Hart, 2006). Of all the chemical measurements made in Yellowstone's hydrothermal waters, it is the contrasting ²⁰⁸Pb/²⁰⁶Pb signatures preserved by these two adjacent hydrothermal features which uniquely require and identify two distinct lithological influences. The elevated ²⁰⁸Pb/²⁰⁶Pb presented by Red Bubbler results from increased interaction with the LCT, which has a high ²³²Th/²³⁸U, while the lower ²⁰⁸Pb/²⁰⁶Pb seen in Perpetual Spouter's waters indicates a stronger influence of the more deeply buried Paleozoic and Mesozoic sedimentary rock units which have a much lower ²³²Th/²³⁸U characteristic of carbonates. We therefore posit that the fluids emanating from Perpetual Spouter are more indicative of the original hydrothermal reservoir hosted in the deep Paleozoic and Mesozoic sedimentary rocks. Whereas the fluids emanating from Red Bubbler, likely began with an isotopic signature like that of Perpetual Spouter, but then post phase separation shallow water-rock interaction with the

volcanic LCT, which has a higher ²³²Th/²³⁸U, imparted a higher ²⁰⁸Pb/²⁰⁶Pb on Red Bubbler's waters.

Amazingly, there have been surprisingly few measurements of radiogenic isotopes in Yellowstone's hydrothermal waters. As such, our isotopic results, particularly ²⁰⁸Pb/²⁰⁶Pb, demonstrate the importance of source lithology and reactive transport for establishing the geohydrobiological feedbacks that ultimately control the bimodal patterns in the Two Pools geochemistry and microbial diversity. Specifically, our ²⁰⁸Pb/²⁰⁶Pb measurements uniquely identify the "deep" hydrothermal aquifer's lithology as sedimentary and not volcanic in character, contrary to what is typically assumed about the lithology of the deep aquifer, and they quantitively demonstrate the extent to which acid-sulfate waters are chemically weathering the near-surface Lava Creek volcanic tuff and inheriting its chemical and isotopic signature. Furthermore, as shown below in our modeling of water rock-interaction timescales, this ²⁰⁸Pb/²⁰⁶Pb fingerprinting is both self-consistent and critical for our reactive transport modeling.

4.4 Two Pools, Two Timescales: (228Ra/226Ra) Chronometer for determining the timescales of Reactive Transport

While reaction-path models can predict the chemical reactions during water-rock interaction, knowledge of the timescales of water-rock reaction and fluid transport are poorly known. Constraining these timescales is critical to understanding the dynamics of these systems. The U- and Th-decay series systematics provide useful Quaternary chronometers (Sims et al., 2021) and can help to determine the duration of water-rock reactions and fluid transport on timescales of tens to hunreds of thousands of years (Kadko and Moore, 1988; Kadko et al., 2007).

Within the U- and Th-decay series (Fig. 4) is a quartet of Ra isotopes with large differences in their half-lives: 226 Ra ($t_{1/2}$ = 1600 years), 228 Ra ($t_{1/2}$ = 5.75 years), 224 Ra ($t_{1/2}$ = 3.63 days) and 223 Ra ($t_{1/2}$ = 11.43 days). These vastly different half-lives, coupled with strong partitioning of Ra into fluid during water-rock reactions, provide a novel chronometer to quantify

the timescales of gas-water-rock interaction in Yellowstone's convective hydrothermal system. Models utilizing Ra isotopes to establish timescales of water-rock interaction have been successfully applied to terrestrial groundwater systems (Krishnaswami et al., 1982), deep ocean hydrothermal systems (Kadko and Moore, 1988), Icelandic hydrothermal waters (Kadko et al., 2007) and Yellowstone's hydrothermal waters (Clark and Turekian, 1990; Sturchio et al., 1993). Remarkably, and of historical significance, in 1906, only ten years after Ra was first discovered and isolated by the Curries at the turn of the twentieth century, scientists for the USGS measured Ra in Yellowstone's thermal waters to determine the "hydrography of the Yellowstone hydrothermal system" (Schlundt and Moore, 1909; Schlundt and Breckenridge, 1938). In this study, we use measurements of ²²⁸Ra and ²²⁶Ra to determine the timescales of water-rock interaction, and measurements of both long-lived ²³⁸U, ²³²Th and ²³⁰Th and short-lived ²²⁴Ra, ²²³Ra and ²²²Rn to constrain model parameters and to test assumptions implicit to the application of the (²²⁸Ra/²²⁶Ra) chronometer.

Conceptually, Yellowstone's convective hydrologic cycle can be broken into four distinct stages.

Stage 1: Meteoric water enters the ground, presumably as recharge from the nearby Madison Plateau and the Absaroka and Gallatin Mountain Ranges (Rye and Truesdell, 1993, 2007; Kharaka et al., 2002; W Payton Gardner et al., 2010; W. Payton Gardner et al., 2010). Shallow groundwater recharge can serve as a diluent, or even as an oxidant, to deep thermal waters; however, meteoric water contains minimal concentrations of both Th and Ra (generally << 1 ppb). Thus, the (228Ra/226Ra) chronometer does not address, nor is it influenced by, the timescales of Stage 1.

<u>Stage 2:</u> The downward percolating groundwater infiltrates Yellowstone's magmaticallyheated rock; these waters chemically react with this hot rock and are infused with magmatic gases rising from below. It is here in the 'deep homogenous hydrothermal reservoir' that high-temperature and high-pressure conditions facilitate fluid-gas-rock interactions. ²⁰⁸Pb/²⁰⁶Pb isotopes indicate that outside the caldera this deep reservoir is made up of Paleozoic and Mesozoic sediments and carbonates. Radium isotopes are transferred from aquifer rocks (made up of either primary or secondary minerals or both) into solution, through both direct rock

dissolution and alpha recoil. Stage 2 is when the clock starts for the (228Ra/226Ra) chronometer.

Stage 3: Upon heating in Stage 2, the chemically-infused near-supercritical water rises relatively quickly to the surface on account of temperature and pressure gradients. Clark and Turekian, 1990 assumed, albeit without direct evidence, that the water rises instantaneously to the surface without time for decay, thus preserving the Ra isotope signal acquired during the time of deep high-temperature water-rock interaction. However, given the short half-life of ²²⁸Ra of 5.77 years, the possibility for some decay of ²²⁸Ra exists and needs to be considered and/or ruled out by other constraints.

<u>Stage 4:</u> The rising water undergoes decompression boiling and separates into an alkaline-chloride fluid phase and a steam-dominated vapor phase. The phase-separated fluids then subsequently mix to various degrees with oxidizing shallow meteoric water. In the case of the Two Pools – these phase-separated waters emerge as the alkaline-chloride Perpetual Spouter and the acid-sulfate Red Bubbler. Importantly, these different compositions cause different degrees of water-rock interaction. Acidic waters corrosively weather the shallow LCT, resetting the chemical and isotopic composition of the water and the Ra chronometer. Alkaline-chloride waters precipitate silica sinter and armor themselves against water-rock interaction, thus preserving a deeper signal.

The differences inferred for fluid sources between Perpetual Spouter and Red Bubbler suggest that timescales of water-rock interaction differ considerably between these two hot springs. Essentially, the isotope data indicate that the water in Perpetual Spouter and Red Bubbler represent two different stages and hydrological regimes in the Yellowstone hydrothermal system (Fig. 3). Perpetual Spouter's alkaline-chloride water represents the deep hydrothermal reservoir that is minimally perturbed by water-rock interaction *en route* to the surface (Nordstrom et al., 2009). Thus, for Perpetual Spouter's alkaline-chloride boiled waters, we interpret our Ra measurements as providing information on the timescales of water-rock interaction in the "deep homogeneous hydrothermal reservoir" (i.e., Stage 2 with perhaps some ²²⁸Ra decay during transport in Stage 3). In Red Bubbler's acid-sulfate waters, water-rock interaction during reactive transport through the LCT resets the composition of the fluids, including its Ra concentrations and isotopes. Thus, with Red Bubbler's waters, the Ra

chronometer provides information on the timescales of recent, shallow water-rock interaction occurring in Stage 4 after phase separation.

Radium nuclides can enter Yellowstone's hydrothermal waters by any combination of the following four processes: (1) dissolution of aquifer solids, (2) *in situ* radioactive decay of the dissolved parent nuclides, (3) direct recoil across the solid-liquid boundary as a result of production by radioactive decay in the solid, and (4) desorption from solid surfaces. Radium nuclides will leave the system by either one of two processes: 1) decay; or 2) adsorption onto a surface. An important assumption implicit within (228Ra/226Ra) chronometer calculations is the assumption that U- and Th-decay series isotopes are in equilibrium in the unaltered aquifer source rock. In our application here, this assumption is initially quite reasonable given that the half-lives of the relevant progeny isotopes (Fig. 4) are very short compared to the ages of both the sedimentary rocks we are positing to be the host of the deep aquifer (the underlying deep sedimentary rocks are late Paleozoic and Mesozoic) and the LCT (640 ka) that the acid-sulfate waters are interacting with. That said, progressive dissolution will disrupt this disequilibrium state in the rock, strip out U preferentially, and ultimately favor the enrichment of shorter-lived nuclides in the fluids, including ²²⁸Ra.

The non-steady state solution describing the activity of a Ra daughter in solution is indicated by A_D^L , and can be calculated from the expression:

888
$$A_D^L = P(1 - e^{-\lambda t})$$
 Eq. 1

Where activity is defined as $n\lambda$, representing the isotope's decay constant, λ , multiplied by the number of atoms, n, of that isotope, and has units of decays per unit time for a given quantity.

Ignoring the effects of adsorption/desorption, the total activity for a Ra isotope in solution can be cast as:

893
$$A_D^L = (P_1 + P_2 + P_3)(1 - e^{-\lambda t})$$
 Eq. 2

Where the production terms (P) for Ra isotopes (atoms • time⁻¹ • kg of water⁻¹) going into Yellowstone's hydrothermal fluid are the algebraic sum of: P₁) *in situ* decay of parental Th

isotopes in solution; P₂) input of Ra from rock alteration and dissolution by corrosive, high-temperature and low pH hydrothermal fluids; and P₃) recoil of Ra isotopes into the fluid from decay of their Th parents in the host rock. Radium loss is mainly through decay and, to a very limited extent, adsorption depending on the composition of the phase-separated fluids. Our formalism, at some peril, ignores the effects of adsorption/desorption. Ignoring the effects of adsorption/desorption is reasonable for Red Bubbler's acidic waters, but potentially problematic for alkaline-chloride waters like Perpetual Spouter, particularly if the process is isotope selective.

Very low Th/Ra in both Red Bubbler and Perpetual Spouter equate to negligible Ra ingrowth from the decay of aqueous parental Th, even in Red Bubbler's acidic waters where Th is slightly soluble (Tables 1 and 3). Thus, the ingrowth production term, P₁, can be omitted, and equation 2 reduces to:

907
$$A_D^L = (P_2 + P_3)(1 - e^{-\lambda t})$$
 Eq. 3

 P_2 , the input of the Ra isotopes (A_D^L) as a result of high-temperature water-rock chemical reactions/dissolution is given by:

910
$$P_2 = A_D^L = \frac{A_P^R}{W \cdot t \cdot \lambda \cdot 10^{-3}} (1 - e^{-\lambda t})$$
 Eq. 4

where A_P^R = activity of parent nuclide in host rock (dpm • g⁻¹) and W = water/rock ratio (g • g⁻¹) which is defined as the number of grams of fluid required to dissolve one gram of rock. The 10^{-3} factor is to account for the rock's activity being given in (dpm • g⁻¹), whereas P_2 is in units of (atoms • time⁻¹ • kg of water⁻¹). Because λ is in the denominator, nuclide input from rock dissolution will be most important for the longer-lived nuclides, thereby producing low (228 Ra/ 226 Ra) relative to the equilibrium rock ratio (Fig. 4 inset). Finally, when W approaches infinity P_2 becomes less significant.

P₃, the recoil rate (R) of a nuclide, is given by the expression:

919
$$P_3 = A_D^L = (R) (1 - e^{-\lambda t})$$
 Eq. 5

Recoil is most important for short-lived nuclides and in isolation this process will produce high (228 Ra/ 226 Ra) (Fig. 4 inset). Of all the production terms, recoil input is one of the most uncertain and difficult to quantify. Most studies use the 222 Rn activity to approximate the recoil supply rate of all alpha decay products (Krishnaswami et al., 1982; Kadko and Moore, 1988; Clark and Turekian, 1990; Kadko and Butterfield, 1998) because 222 Rn is chemically inert and thus not affected by adsorption or other secondary reactions. Furthermore, 222 Rn has a very short half-life ($t_{1/2} = 3.85$ d) and will quickly reach a steady state in solution ($P\lambda = \lambda A$). However, application of 222 Rn as a recoil proxy for Ra isotopes requires the use of a recoil efficiency coefficient of 222 Rn relative to Ra isotopes (expressed here as ε). Measurements of 224 Ra ($t_{1/2} = 3.64$ days) can provide another estimate of the Ra recoil from the aquifer rock into the reacting fluid. 224 Ra has a half-life similar to that of 222 Rn and is produced from the alpha decay of 228 Th ($t_{1/2} = 1.9$ years), which is in turn produced by 228 Ra decay. Since recoil favors isotopes with short half-lives and assuming, reasonably, that very little 228 Th is in solution, the 224 Ra in the circulating fluid is being produced primarily by recoil from rock and is thus another good proxy of recoil.

Summing these two production terms and expressing equation 3 in terms of (²²⁸Ra/²²⁶Ra) activity in the fluid provides the final expression for the Ra chronometer used in this study:

936
$$\left(\frac{^{228}Ra}{^{226}Ra}\right) = \frac{\left[(R^{228}) + \left(\frac{^{(232}Th)^*}{_{10^{-3} \cdot \lambda_{228 \cdot W \cdot t}}}\right)\right] \left(1 - e^{-\lambda_{228}t}\right)}{\left[(R^{226}) + \left(\frac{^{(238}U)^*}{_{10^{-3} \cdot \lambda_{226 \cdot W \cdot t}}}\right)\right] \left(1 - e^{-\lambda_{226}t}\right)}$$
 Eq. 6

When solving equation 6 as a function of time, and under typical conditions where both recoil and dissolution are contributing to the fluid's composition, the functional form of this equation starts with (228 Ra/ 226 Ra) rising rapidly over time to reach an apogee, then quickly decreases over time (Fig. 4 inset). The maximum (228 Ra/ 226 Ra) and the functional form of its decrease over time are controlled by: 1) the relative half-lives of 228 Ra and 226 Ra; 2) (232 Th)/(238 U) in the aquifer source rock; 3) the 228 Ra and 226 Ra recoil rates, R; and, 4) the extent of rock dissolution, which is parametrized as the chemical water/rock ratio, W (g • g⁻¹).

Red Bubbler and Perpetual Spouter waters have strikingly different chemistries and isotopic signatures. A critical feature of this chemical distinction is the vastly different

(²²⁸Ra/²²⁶Ra) between the two pools. Perpetual Spouter has an average (²²⁸Ra/²²⁶Ra) of 5.97 ± 3.09, and Red Bubbler has an average (²²⁸Ra/²²⁶Ra) of 45 ± 6 (Table 2). We argue based upon radiogenic isotopes and geophysical observations that post-phase separation reactive transport processes impart this bimodal geochemical and isotopic difference, with Perpetual Spouter and Red Bubbler providing information on two separate regimes beneath the NGB hydrothermal system. Perpetual Spouter's alkaline-chloride waters are dominated by fluids representing a deep hydrothermal reservoir where water-rock interaction was occurring with Paleozoic and Mesozoic sedimentary rocks, whereas Red Bubbler's acidic waters are dominated by fluids suggestive of shallow water-rock interaction with the LCT. Thus, in the following we consider Perpetual Spouter and Red Bubbler separately when applying the Ra chronometer.

In the following Ra chronometer modeling, we explore reasonable values for the determinant variables: 1) 232 Th/ 238 U of the aquifer source rock, 2) recoil rate (R), and 3) water/rock ratio (W). Justifications for our choice of these variables for each of the two systems, as well as the sensitivity of our results to uncertainties in these variables, is detailed in *Supplementary Material B*.

4.4.1 Application of the Ra Chronometer to Red Bubbler:

Geophysical imaging, combined with geochemical and isotopic data, indicate that Red Bubbler waters (pH \sim 3) represent the mixing of deep hydrothermal waters, vapor phase gases, and shallow oxidizing groundwater flowing in from the adjacent Ragged Hills. Movement of the resulting acidic fluids along their reaction pathway through the LCT significantly weathers the LCT. Red Bubbler's high metal solute concentrations (including U, Ra, and Ba) and its radiogenic Sr and Pb isotopes similar to LCT are evidence of high solute input from shallow water-rock reaction. In Red Bubbler's waters, the Ra chronometer provides information on the timescales of shallow water-rock interaction occurring after phase separation.

Because the Pb, Nd, Sr and Fe isotopic compositions of Red Bubbler's waters are indistinguishable from those of LCT, and because this system is acidic, we model two endmember scenarios: water-rock interaction with unaltered LCT; and, water-rock interaction

with altered LCT, as measured in borehole Y-9 (Sturchio et al., 1993). Because of progressive alteration during water-rock interaction, it is likely that the (²³⁸U/²³²Th) of the aquifer source rock is intermediate to these two endmembers. We also note that in acidic systems, the rock and mineral surfaces are likely to be protonated and thus repellant toward Ra cations; as such, it is reasonable to ignore the effects of adsorption/desorption when calculating the mean timescales of water-rock interaction from Red Bubbler's (²²⁸Ra/²²⁶Ra). Finally, in our modeling, we assume that the non-reactive transport time from the deep reservoir (i.e., once chemical reaction between fluid and rock has ceased) is negligible relative to the half-life of ²²⁸Ra. This assumption is reasonable given the near-surface water-rock interactions that are resetting the (²²⁸Ra/²²⁶Ra) chronometer.

Red Bubbler's (²²⁸Ra/²²⁶Ra) ranges from 37.9 - 50.3 (Fig. 5, Table 2), with an average of 45 ± 6. Assuming that U- and Th-decay series progeny are in equilibrium in the LCT source rock, the (²²⁸Ra/²²⁶Ra) production ratio of LCT (1.7 ± 0.15), is inferred from our measurements of (²³²Th/²³⁸U). This much lower theoretical rock (²²⁸Ra/²²⁶Ra) requires that water-rock interaction processes, namely through recoil, preferentially enrich ²²⁸Ra in the fluid relative to ²²⁶Ra. Thus, Red Bubbler's very high (²²⁸Ra/²²⁶Ra) requires recent and short-lived water-rock interaction with significant ²²⁸Ra input from recoil. This temporal constraint holds for both unaltered and altered LCT.

In these calculations, recoil rate, R, and water/rock ratios, W, are inversely coupled in producing a given (²²⁸Ra/²²⁶Ra). This inverse relationship exists because W is in the denominator of the rock dissolution production term (Eq. 4), so when W values are high, the production term, P₂, becomes increasingly less relevant. There are unique combinations of W and R values capable of producing a given (²²⁸Ra/²²⁶Ra). In Red Bubbler's case we use the maximum (²²⁸Ra/²²⁶Ra) of 50.3 for our modeling. The higher (²³²Th/²³⁸U) of altered LCT requires lower W and R values to produce the high (²²⁸Ra/²²⁶Ra) of Red Bubbler's waters.

For all scenarios and all samples, calculated mean water-rock residence times for Red Bubbler are less than 100 years (Fig. 5a). The different aquifer rock lithologies examined have vastly different (²³²Th/²³⁸U) (Table 3), which has a significant effect on required recoil rates (*Supplementary Material B*), water/rock ratios, the form of the model curves, and calculated

water-rock residence times (Fig. 5a). Average unaltered LCT has a $(^{232}\text{Th}/^{238}\text{U})$ of 1.67 ± 0.15 and calculated water-rock interaction times range from 15 years to 44 years. Altered LCT (based on borehole Y-12) has a much higher $(^{232}\text{Th}/^{238}\text{U})$ of 4.8 because of the much greater solubility of hexavalent U; this higher $(^{232}\text{Th}/^{238}\text{U})$ shallows the form of the model curve resulting in slightly longer calculated mean residence times ranging from ~ 16 years up to 90 years. Intermediate or progressive alteration (and U removal) between unaltered LCT to altered LCT (assuming Y-12 as an endmember) will result in model curves and model ages intermediary between these two endmembers.

Decisively, across a wide range of parameter space, and regardless of whether the aquifer source rock is unaltered or altered LCT (both are consistent with Red Bubbler's Pb isotopes), Red Bubbler's exceptionally high (228Ra/226Ra) requires recent and short water-rock interaction times (<100 years) (Fig. 5a). In the context of Red Bubbler's hydrological regime, this timescale represents the average length of time, post phase separation, that Red Bubbler's waters were sufficiently acidified to start chemically weathering the LCT. We note that this timescale is an average as it integrates across the range of porosities and timescales experienced by the collective emergent waters. However, we also note that the extent of weathering must be significant enough that the isotopic compositions are buffered, as the measured values were constant over the four-year period of our measurements.

4.4.2 Application of the Ra Chronometer to Perpetual Spouter:

Alkaline-chloride waters, such as those emanating from Perpetual Spouter (pH \sim 7.5), precipitate silica sinter along their conduits, which armors against shallow water-rock interaction. Beyond the effects of volatile loss during boiling, alkaline-chloride waters are minimally perturbed *en route* to the surface and are thus posited to represent the deep, homogeneous, hydrothermal reservoir (Nordstrom et al., 2009). Thus, for alkaline-chloride waters, the Ra chronometer provides perspective on the timescales of deep water-rock interaction before phase separation.

Perpetual Spouter's waters have ²⁰⁸Pb/²⁰⁶Pb intermediate between Yellowstone's shallow volcanic rocks (e.g., LCT) and its deep, underlying Paleozoic to Mesozoic sandstones, shales, and limestones. There are three possible explanations for this intermediate ²⁰⁸Pb/²⁰⁶Pb signature.

1) Changing conditions of water-rock interaction. Initially, Perpetual Spouter's source waters interacted with the underlying deep Paleozoic to Mesozoic sediments, and then as these deep waters rose to the surface, they secondarily interacted with the shallow LCT. 2) Mixing of deep and shallow waters. In this scenario, different waters at different depths independently interact with their respective endmember lithologies and then subsequently mix. Perpetual Spouter's deep waters carry the deep sedimentary rock's low ²⁰⁸Pb/²⁰⁶Pb isotopic signature, whereas the shallow waters carry a trace signature of LCT or other regional volcanic rocks. 3) A local dust component of volcanic or nearby plutonic rocks with high ²⁰⁸Pb/²⁰⁶Pb is elevating Perpetual Spouter's ²⁰⁸Pb/²⁰⁶Pb. The very low metal solute content of the Perpetual Spouter waters make all three scenarios possible.

Regardless, and importantly, the ²⁰⁸Pb/²⁰⁶Pb of Perpetual Spouter's waters reflect a geochemical signal that suggests mixing with components from a deep (below LCT) sedimentary rock-hosted aquifer. These sedimentary rocks have low U and Th concentrations and very low (232Th/238U), in contrast to the local volcanic rocks, in particular the LCT, that have higher U and Th concentrations and much higher (232Th/238U). Therefore, using the U and Th abundances of the sedimentary rocks makes it possible to model the timescales of Perpetual Spouter's waterrock interaction by using the Ra chronometer. This is in stark contrast to the earlier modeling of Clark and Turekian (1990), who, in the absence of radiogenic isotopic data, assumed that the cations, including Ra, in all Yellowstone hydrothermal fluids were derived from average volcanic rock. There are several possible local sedimentary rock units, or even a combination of them, that can serve as the deep aguifer represented by Perpetual Spouter's waters. Their [U], [Th] and (²³²Th/²³⁸U) are tabulated in Table 3. Because of our lack of knowledge of the specific sedimentary rocks that are hosting deep aquifer reservoir(s), and several of them could be involved, we calculated an average Paleozoic-Mesozoic sedimentary rock composite for modeling purposes using the average [U], [Th] and (232Th/238U) values from Sturchio et al., 1993.

Perpetual Spouter's (228 Ra/ 226 Ra) ranges from 2.5 - 8.41, with an average of 5.97 \pm 3.09 (Fig. 5b, Table 2). This range encompasses the (228 Ra/ 226 Ra) values measured by Clark and Turekian, 1990 in three other NGB alkaline-chloride hot spring waters, all reported as pH = 7

1061 (Hydrophane = 2.50 (\pm 0.49); Medusa = 3.89 (\pm 0.29); and Opalescent Springs = 4.43 (\pm 0.70); average of 3.61 (\pm 1.00)).

1063

1064

1065

1066

1067

1068

1069

1070

1071

1072

1073

1074

1075

1076

1077

1078

1079

1080

1081

1082

1083

1084

1085

1086

1087

1088

1089

For alkaline-chloride systems, Clark and Turekian, 1990 assumed that, in the deep system, ²²⁸Ra and ²²⁶Ra are in equilibrium between the solution and the adsorbed phase and that these waters then ascend rapidly to the surface unperturbed by subsequent processes. While it is likely that the different Ra daughters reached equilibrium in the deep sedimentary rock aquifer, changing conditions during fluid ascent, including phase separation and mixing with shallow groundwater, disrupt this equilibrium steady-state. Thus, it is likely that Ra is being deposited/adsorbed (Sturchio et al., 1993) in the near-surface environment and that such effects need to be considered in calculated water-rock interaction timescales.

Fortunately, our measurements of (224Ra/222Rn) in Perpetual Spouter's waters provide a quantitative measure of Ra adsorption/precipitation. Both ²²⁴Ra and ²²²Rn have short and similar half-lives; therefore, both nuclides will be recoiled at a rate similar to their production ratio, as inferred from the (²³²Th/²³⁸U) of the source aguifer. Perpetual Spouter's (²²⁴Ra/²²²Rn) is about an order of magnitude lower than the (²³²Th/²³⁸U) of regional sedimentary or volcanic rock lithologies, including composites (*Table 3*). This apparent depletion of (²²⁴Ra/²²²Rn) relative to its inferred production ratio suggests Ra loss, perhaps in part due to the incorporation of Ra into silica sinter during its deposition. The effect that adsorption and precipitation processes will have on calculated mean water-rock interaction ages depends entirely on whether these shallow processes are altering the (228Ra/226Ra) established in the deep reservoir during stage 2. If 228Ra and ²²⁶Ra are being precipitated and adsorbed in their relative isotopic abundances, the (228Ra/226Ra) will remain unchanged and calculated residence times will remain unperturbed. However, if ²²⁸Ra equilibrates faster with the mobile pool than does ²²⁶Ra (Sturchio et al., 1993), the fluid's (²²⁸Ra/²²⁶Ra) will increase, and the calculated mean water-rock interaction times will appear to be shorter. Consequently, for Perpetual Spouter, the calculated water-rock interaction times should be considered minimum values.

For our calculations of mean water-rock interaction timescales for Perpetual Spouter, we examine: three lithologies – average sediment, unaltered LCT, and altered LCT (not shown); two water/rock ratios, W = 250 and W = 125; and, two recoil rates, R = 500 dpm/l and 1,000 dpm/l

1090 (See Supplementary Material B for discussion of parameter choices and sensitivity analyses). 1091 Calculated mean water-rock residence times for Perpetual Spouter are greater than 100 years for 1092 all scenarios and all samples (Fig. 5b). The various aguifer rock lithologies examined have vastly different (232Th/238U) (Table 3), which has the most significant effect on determining the fluid 1093 (²²⁸Ra/²²⁶Ra) and resulting calculated water-rock residence times (Supplementary Material B). 1094 1095 Changing R and W across the range chosen has a smaller effect on calculated residence times (Fig. 5b). Average Mesozoic sediment has the lowest (²³²Th/²³⁸U) of 0.695, and the shortest 1096 1097 calculated mean residence times for Perpetual Spouter waters, ranging from ~125 years to ~530 years. Average unaltered LCT has a considerably higher (232 Th/ 238 U) of 1.67 (\pm 0.15), requiring 1098 longer residence times of ~330 years to roughly 1,500 years. Altered LCT (Y-12) has an even 1099 higher (232Th/238U) of 4.8 (Sturchio et al., 1993) and requires even longer calculated mean 1100 residence times of ~1,500 years to ~1,800 years for Perpetual Spouter. Note that in this later case 1101 the age is indeterminant for sample Perpetual Spouter #140917, as the fluid (228Ra) is 1102 below the calculated steady-state (228Ra/226Ra) productivity ratio as inferred from the altered 1103 LCT (²³²Th/²³⁸U) of 4.8. Because the ²⁰⁸Pb/²⁰⁶Pb isotope ratios suggest that Perpetual Spouter 1104 1105 waters are best modeled as mixtures of waters that have come from the deeper underlying 1106 Paleozoic to Mesozoic sedimentary rocks (Fig. 5b) with waters that have interacted with LCT (or 1107 other Yellowstone volcanic units), Perpetual Spouter's water-rock interaction timescales are also 1108 likely intermediate between these two endmembers.

These calculations ignore the effects of adsorption/desorption or coprecipitation on (228Ra/226Ra). If, during Ra precipitation or adsorption, 228Ra equilibrates faster with the mobile pool than does 226Ra (Sturchio et al., 1993), the fluid's (228Ra/226Ra) will increase, and the calculated mean water-rock interaction times will appear to be shorter and would be considered *minimum* values/ages. However, if the time of ascent in Phase 3 is long relative to the half-life of 228Ra, then the fluid's (228Ra/226Ra) will decrease, and the calculated mean water-rock interaction times would be considered *maximum* values/ages.

1109

1110

1111

1112

1113

1114

1115

1116

1117

1118

1119

Nonetheless, Perpetual Spouter's low (²²⁸Ra/²²⁶Ra) indicates a mean water-rock interaction time of hundreds to thousands of years (Fig. 5b), consistent with Perpetual Spouter waters coming from Yellowstone's deep hydrothermal system where the waters were interacting with the underlying Paleozoic and Mesozoic sediments (Fig. 3b). These time constraints for

Perpetual Spouter are consistent with, but much more definitive than, tritium constraints that only define Perpetual Spouter waters to be dominantly (>93%) tritium-free (Pearson and Truesdell, 1978; Gardner et al., 2011) and thus predominantly pre-1945 (i.e., pre-bomb) (Cauquoin et al., 2016). Ultimately, it is not surprising that Yellowstone's deep hydrothermal water has a convective timescale of several hundreds of years. However, given the high outflux of alkaline-chloride water, and the high recharge into the Yellowstone hydrothermal system from the Madison Plateau and the Absaroka and Gallatin Mountain Ranges, it seems unlikely that these waters' reaction times are thousands to tens of thousands of years old (Rye and Truesdell, 1993, 2007; Kharaka et al., 2002; W Payton Gardner et al., 2010; W. Payton Gardner et al., 2010).

In summary, this study is the first-time anyone has determined the timescales of waterrock interaction, focusing on phase-separated waters. The observed high ²²⁸Ra/²²⁶Ra in Red Bubbler's acid-sulfate waters requires recent and short, shallow water-rock interaction timescales (10s of years) coming from a reservoir with high (²³²Th/²³⁸U), whereas Perpetual Spouter's neutral chloride waters, which are coming from the deep hydrothermal reservoir with low (²³²Th/²³⁸U), have much older ages and longer water-rock interaction time scales (100's-1,000's of years). Establishing the timescales of water-rock interaction is an important and hard-to-determine parameter in natural systems, yet it is a critical component of the Domköhler number for reactive transport. Demonstrating the viability of the ²²⁸Ra/²²⁶Ra chronometer used here is important for understanding phase separation in Yellowstone's hydrothermal system and has applicability across a range of groundwater and hydrothermal studies.

4.4 Two Pools, Two Taxonomically and Functionally Distinct Communities

Phase separation and its influence on reactive transport and the chemistry of springs has a profound effect on the taxonomic and functional composition of their resident microbial communities, as revealed here for Red Bubbler and Perpetual Spouter (Fig. 6), which are representative of broader Yellowstone-wide variation in microbial communities (Fig. 7). The planktonic and sediment communities from Red Bubbler were comprised entirely of Archaea, consistent with previous studies indicating that Archaea dominate the most acidic and highest temperature springs in Yellowstone (Inskeep et al., 2013; Colman et al., 2018) and in other

globally distributed continental geothermal systems for instance in New Zealand, Iceland, China, and Japan (Hou et al., 2013; Ward et al., 2017; Colman et al., 2023). In contrast, dominant planktonic and sediment populations in Perpetual Spouter comprised both Archaea and Bacteria. This set of observations is attributed to the combination of high temperature and acidity that together impose chronic stress on microbial cells, a condition that has been suggested to select for Archaea over Bacteria during the assembly of those communities (Valentine, 2007; Colman et al., 2018). The combination of high temperature and acidity is also likely responsible for the lower taxonomic diversity associated with Red Bubbler, as has been suggested for other acidic hot springs in Yellowstone (Inskeep et al., 2013; Colman et al., 2018; Fernandes-Martins et al., 2023) and other globally distributed acidic springs (Power et al., 2018; Colman et al., 2023).

Previous studies suggest that the acidification of hot springs in Yellowstone is driven by a series of geobiological feedbacks that involve both abiotic and biotic components (Mosser et al., 1973; Nordstrom et al., 2005, 2009; Colman et al., 2018). H₂S, which is enriched in vapor phase gases that source acidic springs, can be oxidized abiotically at high temperature by oxygen that is made available by mixing with recently infiltrated meteoric water (Brock et al., 1972; White et al., 1988; Colman et al., 2018). Abiotic oxidation of H₂S generates S₂O₃²⁻ (Eq. 5), which is unstable in waters with pH <6.0 (Xu and Schoonen, 1995) and rapidly disproportionates to form sulfite (HSO₃⁻) and S⁰ (Eq. 6) (Nordstrom et al., 2005), the latter of which accumulates due to its low solubility and slow reactivity with water at temperatures of <100°C (Nordstrom et al., 2005).

1169	$2HS^{-} + 2O_{2} \rightarrow S_{2}O_{3}^{2-} + H_{2}O$	Eq. 5
1170 1171	$H^+ + S_2O_3^{2-} \rightarrow S^0 + HSO_3^{-}$	Eq. 6
1172	2 0	24. 0
1173	$HSO_3^- + 1/2O_2 \rightarrow SO_4^{2-} + H^+$	Eq. 7
1174 1175	$S^0 + 3/2O_2 + H_2O \rightarrow SO_4^{2-} + 2H^+$	Eq. 8

 HSO_3^- is also unstable at high temperature in the presence of oxygenated waters with a pH < 4.0 (Colman et al., 2020) and oxidizes abiotically to form SO_4^{2-} via Eq. 7 (Nordstrom et al., 2005). Importantly, these abiotic reactions (Eqs. 5-7) do not generate net acidity, since a mol of H^+ is consumed in Eq. 6 and a mol of H^+ is generated in Eq. 7. Rather, it is the O_2 -dependent oxidation of S^0 (Eq. 8) that is responsible for the generation of acidity and microbial activity mediates this

process at temperatures of <100°C (Mosser et al., 1973). The functional capabilities of dominant populations in Red Bubbler, which importantly allow for O₂-dependent oxidation of S⁰ (Fig. 6b), is consistent with this model for hot spring acidification. As spring acidification progresses, the stabilities of intermediate H₂S oxidation products (S₂O₃²⁻ and HSO₃⁻) continue to decrease, thereby increasing the amount of S⁰ available for additional acid generation. These geobiological feedbacks are responsible, at least in part, for the unique chemistry and biology associated with Red Bubbler and that differentiate them from Perpetual Spouter, and more broadly, the bimodal differentiation of hot spring microbial ecosystems observed across Yellowstone and elsewhere (Fig. 7) (Inskeep et al., 2013; Hou et al., 2013; Power et al., 2018; Moreras-Marti et al., 2021; Colman et al., 2023). The enrichment for aerobic S⁰ oxidation metabolic potential in metagenomes from a variety of acidic high temperature hot springs in Yellowstone (Colman et al., 2019) indicates that this geobiological feedback is responsible for the bimodal distribution of spring pH across Yellowstone, and one that is established upon the foundation of phase separation and reactive transport processes described above.

A comparison of the taxonomic and functional composition of planktonic and sediment communities in Red Bubbler when compared to those of Perpetual Spouter points to another striking consequence of phase separation and reactive transport on the assembly of microbial communities in hot springs. Whereas communities from Red Bubbler exhibited similar functional compositions, but distinct taxonomic compositions, those from Perpetual Spouter were far more differentiated at a functional level (Fig. 6c). Previous work has shown that plankton and sediment communities in hot springs are often differentiated at a taxonomic level, with the presence of solid phase minerals in sediments and greater access to infused atmospheric oxygen in waters suggested to be the predominant reasons for this differentiation (Colman et al., 2016; Fernandes-Martins et al., 2021). From a deterministic perspective on community assembly, there are only two logical mechanisms that could lead to this observed differentiation between planktonic and sediment communities in hot springs: 1) adaptations that allow organisms to better compete for nutrients with differential availability in the water column versus sediments of springs, as described above; or, 2) sourcing of planktonic cells from the subsurface at a rate that exceeds the growth rate of cells adapted to conditions in the hot spring waters. We believe that both mechanisms are at play, with mechanism-one being more important in

1211 differentiating communities inhabiting circumneutral to alkaline springs and mechanism-two 1212 being more important in differentiating communities inhabiting vapor phase-sourced springs. As 1213 mentioned above, Perpetual Spouter is likely sourced by water from the deep hydrothermal 1214 reservoir, with transport times estimated to be on the order of hundreds of years. The long 1215 residence time of these waters in the deep reservoir allow for extensive interaction with minerals 1216 in the bedrock that hosts this aquifer, which drives the system to anoxia. Those fluids are often 1217 also enriched in As(III), leached from rhyolite bedrock that hosts the hydrothermal aquifer 1218 (Stauffer and Thompson, 1984; McCleskey et al., 2022a). Furthermore, the conduits feeding 1219 deep hydrothermal water to circumneutral to alkaline springs like Perpetual Spouter are armored 1220 by precipitated silica (Vitale et al., 2008; Gibson and Hinman, 2013), a feature that would be 1221 expected to prevent extensive infusion of oxidized meteoric fluids that have recently infiltrated 1222 the surface. In effect, this would limit the chemical reactions that can support microbial 1223 metabolism to those that are less dependent on O₂ from atmospheric influx due to its low 1224 solubility of O₂ at high temperatures (Amend and Shock, 2001). The dominant organism within 1225 the Perpetual Spouter community was affiliated with the currently uncultivated Ca. Calditenuis 1226 aerorheumensis (Caldarchaeales), an organism that is inferred based on metagenomic data to be 1227 facultatively aerobic and facultatively autotrophic. Metabolic inference suggests that these 1228 organisms may be able to fuel autotrophic energy metabolism via oxidation of carbon monoxide 1229 or sulfide coupled potentially to As(V) or O₂ reduction. The apparent ability of the dominant Perpetual Spouter population in waters and sediments to switch between aerobic (O₂ reduction) 1230 1231 and anaerobic (e.g., As(V) reduction) respiratory strategies may be a consequence of the low and 1232 possibly variable levels of O₂ in high temperature waters of circumneutral to alkaline springs. 1233 Importantly, the amount of total arsenic as arsenite (As(III)) in circumneutral to alkaline springs 1234 tends to be >50%, although it can be as high as 100% (Stauffer and Thompson, 1984; 1235 McCleskey et al., 2005, 2014, 2022a,b). The total amount of arsenic in Perpetual Spouter was 1236 nearly a factor of 3 greater than that of Red Bubbler, and ~50% of this was as As(V) 1237 (Supplemental Materials Table S1). It is possible that conversion of As(III) to As(V) is catalyzed 1238 via co-inhabiting *Thermocrinis* populations whose MAGs encode As(III) oxidizing capability. 1239 The apparent abilities of many other populations in Perpetual Spouter to utilize arsenic 1240 compounds as reductants (e.g., As(III); Thermocrinis) or oxidants (e.g., As(V); Ca. Calditenuis 1241 aerorheumensis) may also reflect the adaptations of microbial populations to survive in hot

springs sourced by the deep hydrothermal aquifer. The lack of such an ability in the Red Bubbler populations may conversely reflect differences in fluid sourcing and reactive transport between the Two Pools, which exerts primary influence on their geochemistry and thus the availability of more thermodynamically preferable substrates (e.g., iron and sulfur compounds) (Shock et al., 2010) to fuel microbial metabolism. Cultivation of the Caldarchaeales populations and additional investigation of arsenic metabolism in this and other lineages would allow confirmation of their ability to carry out metabolisms predicted based on analyses of their MAGs.

1242

1243

1244

1245

1246

1247

1248

1249

1250

1251

1252

1253

1254

1255

1256

1257

1258

1259

1260

1261

1262

1263

1264

1265

1266

1267

1268

1269

1270

1271

In contrast to Perpetual Spouter, the fluids that source Red Bubbler are channeled through a diffuse transport network, as shown by near surface geophysical measurements reported herein. This diffuse flow allows for mixing of reduced fluids (gases) with recently infiltrated oxidized meteoric waters, which would be expected to support microbial activity if other conditions (e.g., temperature constraints) are met (Shock and Holland, 2007; Shock et al., 2010). Despite the ephemeral nature of Red Bubbler, as described above, it was flowing during the time that samples for molecular analyses were collected. As such, the observed taxonomic disparity, coupled with the limited residence time associated with Red Bubbler waters during the time of sample collection, point to the dominant MAG in the planktonic phase (Sulfolobales 'Acd1') as possibly being sourced from the subsurface of this spring, rather than being specifically adapted to localized conditions in the water column. Consistently, a recent analysis of subsurface waters in another spring within the NGB, Cinder Pool, demonstrated that the Sulfolobales Acd1 group increased in abundance with waters at depth (up to 21 m) relative to surface waters (Colman et al., 2022). In support of this argument, it is unlikely that stark chemical differences (e.g., acidification of meteoric water by nearly four orders of magnitude) can develop between the sediment and water column on such a short time scales of fluid residency in Red Bubbler. Nonetheless, and as stated above, metabolic reconstruction of the dominant archaeal populations in both the planktonic and sediment communities in Red Bubbler indicate that they are supported largely by oxidation of reduced sulfur compounds suggesting that they share the same metabolic niche. We envision that abiotic (or potentially biotic) oxidation of sulfide in the near subsurface of Red Bubbler drives the deposition of S⁰ along the diffuse transport network that sources this spring. The Sulfolobales 'Acd1' population can oxidize this S⁰ in the subsurface to generate acidic waters that emanate from the source of this spring; Sulfolobales 'Acd1' sequences

recovered in the plankton phase of Red Bubbler are thus attributed to sloughed subsurface cells. We suggest that this is due to physiological adaptations (e.g., temperature) that delineate the distribution of taxonomically distinct and functionally equivalent archaeal taxa to different ecological compartments (subsurface vs. surface). Additional physiological studies, including those with cultured Sulfolobales 'Acd1' cells that dominant waters versus Sulfolobales 'QEFN01-2' cells that dominates sediments, will help to assess this intriguing hypothesis.

1272

1273

1274

1275

1276

1277

1278

1279

1280

1281

1282

1283

1284

1285

1286

1287

1288

1289

1290

1291

1292

1293

1294

1295

1296

1297

1298

1299

1300

1301

Finally, the acidification of near surface ground waters as they are transported through the diffuse transport network that sources Red Bubbler is responsible for enrichment of those waters with iron (6.7 to 7.7 mg L⁻¹), the majority (>75%) of which is in a reduced state (Supplemental Materials Table SI) that, based on Fe isotopic data presented here, is leached from local LCT. The outflow channel is lined with iron oxyhydroxides (Fig. 1B) suggesting rapid oxidation and precipitation of iron oxyhydroxides iron. In waters with pH of < 4.0, such as those in Red Bubbler, Fe(II) oxidation with oxygen is slow and requires a microbial catalyst (Edwards et al., 1999). The presence of Archaea in the sediments of Red Bubbler that encode homologs of enzymes that allow for Fe(II) oxidation (e.g., sulfocyanins) to support their energy metabolism is thus attributable to acid leaching of this reduced metal by fluids in the near surface during their transport toward the spring source. Indeed, the dominant Sulfolobales population in Red Bubbler sediments appears to at least partially support primary productivity through aerobic Fe(II) oxidation (Fig. 6b). Leaching of Fe and its availability to support microbial activity in Red Bubbler is enabled by the process of phase separation that allows for the concentration of H₂S in vapor phase gas that is then oxidized through a series of geobiological feedbacks that drive fluid acidification. The absence of homologs involved in Fe(II) oxidation in abundant Perpetual Spouter populations is thus attributed to the lack of Fe(II) in those waters (0.06 mg L⁻¹; Supplemental Materials Table S1) due to the insolubility of iron at circumneutral pH, its instability in the presence of oxygen at circumneutral pH, and the limited water-rock interactions that these fluids experience during their transport to the surface, as outlined in previous sections.

While these results describe the specific communities of Red Bubbler and Perpetual Spouter, they are reflective of other microbiological observations across Yellowstone hot springs (Fig. 7) (Meyer-Dombard et al., 2005; Boyd et al., 2013; Inskeep et al., 2013; Colman et al., 2018, 2019) which have demonstrated stark differences in the taxonomic and functional

compositions of communities in hot springs with varying pH (i.e., due to phase separation). The communities of high-temperature acid-sulfate springs are comprised almost entirely of aerobic sulfur-metabolizing Archaea (Inskeep et al., 2013; Colman et al., 2018; Power et al., 2018) that are supported by functionalities that may be responsible for the acidification of those springs (Colman et al., 2018, 2019). In particular, microorganisms are the catalysts that drive the oxidation of S⁰, which results from incomplete oxidation of H₂S and which is otherwise stable in the absence of biology at temperatures of <100°C (Nordstrom et al., 2005). In contrast, hightemperature alkaline-chloride springs host communities comprising both archaeal and bacterial members (Meyer-Dombard et al., 2011; Inskeep et al., 2013; Fernandes-Martins et al., 2021) that are largely supported by aerobic and anaerobic metabolisms that can involve a variety of different electron donors including arsenate (Fernandes-Martins et al., 2021) that is leached from rhyolite and is enriched in this water type (Stauffer and Thompson, 1984; McCleskey et al., 2022a). Per the phase separation model and for reasons outlined above, the lack of fluid mixing on diffuse flow paths sourcing springs like Perpetual Spouter, combined with the limited availability of O₂ and/or H₂S in those fluids, does not promote enrichment of sulfur-oxidizing populations and the acidification of spring waters.

5. Summary:

Alexander von Humboldt profoundly stated in 1863, that "Everything is Interconnected" (von Humboldt, 1863). Our combined, multi-disciplinary measurements, from the two adjacent, phase-separated pools, Red Bubbler and Perpetual Spouter, provide, for the first time, a four-dimensional (spatial and temporal) understanding of the interconnectedness between hydrological, geochemical, and biological processes occurring before, during and after phase separation (Fig. 8). We uniquely show that Perpetual Spouter's alkaline-chloride waters preserve a signal of deep, protracted (hundreds of years) water-rock interaction with underlying Paleozoic and Mesozoic sedimentary rocks; whereas, in Red Bubbler's acid-sulfate waters, this deep, sedimentary geochemical signal is overprinted by shallow, ongoing, reactive transport with the LCT. Further, near-surface geophysical measurements indicate shallow meteoric recharge is integral in establishing the geobiological feedbacks that oxidize and acidify Red Bubbler's acid-

sulfate waters and promote shallow, ongoing water-rock interaction and chemical weathering; whereas, Perpetual Spouter's alkaline-chloride waters host both aerobic and anaerobic communities that largely reflect the influence of the deeper, anaerobic hydrothermal waters.

1332

1333

1334

1335

1336

1337

1338

1339

1340

1341

1342

1343

1344

1345

1346

1347

1348

1349

1350

1351

1352

1353

1354

1355

1356

1357

1358

1359

1360

1361

Our geophysical and isotopic data highlight causal links between subsurface geological processes and the assembly and diversification of thermophilic microbial communities. As indicated by our near-surface geophysical measurements (Figs. 2b-f), gasses that source the acidic Red Bubbler are channeled through a diffuse transport network and experience significant mixing with near-surface, oxidized groundwaters. Thus, our geophysical imaging supports a model where diffuse flow promotes mixing of reduced fluids (vapor phase gases) with recently infiltrated, oxidized meteoric waters. At this point, and in the subsurface, both abiotic and biotic processes convert the trace vapor phase H₂S and its condensed derivatives (i.e., native sulfur (S⁰) and sulfide minerals) to sulfuric acid, which creates an environment where reactive transport chemically weathers the rock. The resulting shallow chemical weathering is so significant that the fluid's radiogenic and Fe isotopic compositions are identical to the LCT. Furthermore, per the ²²⁸Ra/²²⁶Ra measurements, all of these shallow and coupled abiotic and biotic processes, which ultimately lead to significant chemical weathering of the LCT, are occurring on a timescale of tens of years, and enrich spring waters with Fe(II) that can serve as an electron donor for microbial metabolism and also fuel community productivity. Microbially catalyzed oxidation of this Fe(II) results in the formation of the extensive iron oxyhydroxides that line the outflow channels of Red Bubbler and many other acidic springs in Yellowstone. Thus, our data indicate that the recent, extensive chemical weathering of the LCT, which occurs during reactive transport of acidic waters generated by biotic and abiotic oxidation of sulfur compounds, also create ecological niches through what can be termed niche construction (Colman et al., 2018), highlighting the importance of biotic and abiotic reactions, and feedbacks among them, in supporting and generating the diversity of microbial communities in hot springs.

Our isotopic data also provide insight into the observation that circumneutral to alkaline springs, such as Perpetual Spouter, host both aerobic and anaerobic populations, many of which are dependent on heterotrophic metabolism (Fernandes-Martins et al., 2021). We argue, based upon the ²⁰⁸Pb/²⁰⁶Pb isotopes and existing ³H data, that Perpetual Spouter waters are a mixture of predominantly deep anoxic waters with limited, shallow, oxidized ground waters, plus or minus

dust components. The deep hydrothermal waters are anoxic because long water-rock interaction timescales in the deep sedimentary reservoir (Figs. 3b and 5) promotes extensive oxidation of the host bedrock minerals, driving the hydrothermal waters to become anoxic. Once phase separation has occurred, this anoxic alkaline-chloride water travels through conduits armored by precipitated silica that inhibits extensive infusion of oxidized meteoric fluids, thereby fostering communities capable of anaerobic metabolism. However, the ³H data (Pearson and Truesdell, 1978; Gardner et al., 2011) also require roughly 7% mixing of shallow groundwaters. Furthermore, Perpetual Spouter's slightly elevated ²⁰⁸Pb/²⁰⁶Pb (Fig. 3b), relative to the ²⁰⁸Pb/²⁰⁶Pb in the purported deep sedimentary reservoir, requires a mixing component that could be either water that has interacted with the LCT, or dissolution of dust that influences the water's composition. If dust is the primary contributor to the ²⁰⁸Pb/²⁰⁶Pb signal then this result has implications for nutrient supplies including organic carbon and phosphorous (Aarons et al., 2017; Aciego et al., 2017), possibly from microbial necromass. This might help to explain the prevalence of putative heterotrophs in Perpetual Spouter. In any case, the ³H and ²⁰⁸Pb/²⁰⁶Pb data demonstrate that Perpetual Spouter is a mixture of mostly deep anoxic waters and some shallow oxidized water having nucleogenic ³H and some component (dust or water) with higher ²⁰⁸Pb/²⁰⁶Pb than inferred for the deep hydrothermal sedimentary reservoir. As a result, the table is set for both anaerobic and aerobic heterotrophic populations in circumneutral to alkalinechloride springs.

Our results here represent a seminal example of interconnectedness within a continental hydrothermal system. When examined as an interconnected geohydrobiological system, our data illuminate the geochemical consequences of reactive transport processes and shallow meteoric recharge on the diversification and maintenance of thermophilic microbial communities that inhabit surface and near-surface ecological niches along the fluid flow-paths of this phase-separated hydrothermal system. To this end, our collective results provide unique and direct evidence of the causative connections between subsurface geological processes and biological diversification. And, as such, our integration of different, yet complementary, geological, geophysical, geochemical, and molecular microbial data informs a unique and holistic interpretation of the development and evolution of phase-separated hydrothermal systems in a way not possible by any single method of study (Fig. 8).

While our results are specific to Yellowstone they are of global significance. Phase separation is a universal process in hydrothermal systems that have acted as critical evolutionary hot spots driving the diversification of early life on Earth. Yellowstone hosts the world's largest and most quintessential surface expression of a continental hydrothermal system. Thus, by extrapolation, our study's intellectual advances apply to most hydrothermal systems on Earth and likely throughout the solar system. As such, this research reaches far beyond the interest of any single discipline and speaks to a broader understanding of Earth system science.

Finally, we speculate that these same processes are likely to have taken place in continental hydrothermal systems throughout Earth history, albeit the role of O₂ in hot spring acidification is likely more recent (Andersen et al., 2015).

ACKNOWLEDGEMENTS

This work was conducted under the Yellowstone National Park Research Permit Office with permits: Geochemistry permit Yell-05840 (Sims) and Geophysics permit Yell-06090 (Sims) and Geobiology permit Yell- 05544 (Boyd). The research was supported by grants from the UW Shlemon Center for Quaternary Research, UW-NPS, and UW-FGIA to KWWS, CSS to SRS, and the National Science Foundation (OCE-1260079 and NSF-OCE-1634669 to KWWS; EAR-1820658 to DRC and ESB), NASA (Exobiology NNX16AJ61G to ELS), and the W.M. Keck Foundation (ESB). The Department of Energy Joint Genome Institute's Community Sequencing Program (CSP 504081 to DRC, KWWS, and ESB) supported generation of some of the metagenomic sequence data and analyses used in this manuscript. Erin Phillips, Matt Provart, James St. Clair, Allen Sisel, Jacob Yelton, and Mike McClure are acknowledged for their help with the field work to collect the Geophysical data. JoAnn Holloway is gratefully recognized for helpful suggestions during USGS review of this manuscript as are two anonymous GCA reviewers. Cin-Ty Lee is acknowledged for his enthusiastic support of our research and this paper. GCA's Associate Editor Magdalena Osburn and Executive Editor Jeffrey G. Catalano are gratefully acknowledged for their time and efforts handling this manuscript. Note that any use of trade, firm, or product names is for descriptive purposes only and does not imply endorsement by the U.S. Government.

Appendix A: Supplementary Materials. Supplementary Materials contains two sections.

Supplementary Materials A focuses on the minor observations, interpretations, measurement details and caveats that constrain our interpretation of the near-subsurface geologic features with Geophysical Imaging. **Supplementary Materials B** examines the sensitivity of the $(^{228}\text{Ra}/^{226}\text{Ra})$ chronometer to the determinant variables: 1) the relative half-lives of ^{228}Ra and ^{226}Ra ; 2) $(^{232}\text{Th})/(^{238}\text{U})$ in the aquifer source rock; 3) the ²²⁸Ra and ²²⁶Ra recoil rates, R; and 4) the chemical water/rock ratio, W. In this supplement we also discuss our assumptions, logic and methodologies used to determine these variables, and their associated uncertainties. Data Availability: Research Data "Research Data associated with this article can be accessed at Sims et al. 2023 https://doi.org/ 10.5281/zenodo.8277360

1441 REFERENCES

- Aarons S. M., Blakowski M. A., Aciego S. M., Stevenson E. I., Sims K. W. W., Scott S. R. and Aarons C. (2017) Geochemical characterization of critical dust source regions in the American West. *Geochim Cosmochim Acta* **215**, 141–161.
- Aciego S. M., Riebe C. S., Hart S. C., Blakowski M. A., Carey C. J., Aarons S. M., Dove N. C.,
 Botthoff J. K., Sims K. W. W. and Aronson E. L. (2017) Dust outpaces bedrock in nutrient
 supply to montane forest ecosystems. *Nat Commun* **8**.
- Allen E. T. and Day A. L. (1935) *Hot Springs Of Yellowstone National Park.*, Carnegie Institute of Washington, Washington.
- Alneberg J., Bjarnason B. S., De Bruijn I., Schirmer M., Quick J., Ijaz U. Z., Lahti L., Loman N. J., Andersson A. F. and Quince C. (2014) Binning metagenomic contigs by coverage and composition. *Nat Methods* 11, 1144–1146.
- Amend J. P. and Shock E. L. (2001) Energetics of overall metabolic reactions of thermophilic and hyperthermophilic Archaea and Bacteria. *FEMS Microbiol Rev* **25**, 175–243.
- Andersen M. B., Elliott T., Freymuth H., Sims K. W. W., Niu Y. and Kelley K. A. (2015) The terrestrial uranium isotope cycle. *Nature* **517**, 356–359.
- 1457 Anon (1972) Geologic map of Yellowstone National Park.
- Binley A. (2015) Tools and Techniques: DC Electrical Methods. In *Treatise on Geophysics* (ed. G. Schubert). Elsevier. pp. 233–259.
- Bouligand C., Hurwitz S., Vandemeulebrouck J., Byrdina S., Kass M. A. and Lewicki J. L.

 (2019) Heat and Mass Transport in a Vapor-Dominated Hydrothermal Area in Yellowstone
 National Park, USA: Inferences From Magnetic, Electrical, Electromagnetic, Subsurface
 Temperature, and Diffuse CO₂ Flux Measurements. *J Geophys Res Solid Earth* 124, 291–
 309.
- Boyd E. S., Hamilton T. L., Wang J., He L. and Zhang C. L. (2013) The role of tetraether lipid composition in the adaptation of thermophilic archaea to acidity. *Front Microbiol* **4**.
- Brock T. D. (1971) Bimodal distribution of pH values of thermal springs of the world. *Geol Soc Am Bull* **82**, 1393–1394.
- Brock T. D., Brock K. M., Belly R. T. and Weiss R. L. (1972) Sulfolobus: A new genus of sulfur-oxidizing bacteria living at low pH and high temperature. *Arch Mikrobiol* **84**, 54–68. Cauquoin A., Jean-Baptiste P., Risi C., Fourré E. and Landais A. (2016) Modeling the global
 - Cauquoin A., Jean-Baptiste P., Risi C., Fourré E. and Landais A. (2016) Modeling the global bomb tritium transient signal with the AGCM LMDZ-iso: A method to evaluate aspects of the hydrological cycle. *J Geophys Res* **121**, 12,612-12,629.
- 1474 Chang W. L., Smith R. B., Farrell J. and Puskas C. M. (2010) An extraordinary episode of 1475 Yellowstone caldera uplift, 2004-2010, from GPS and InSAR observations. *Geophys Res* 1476 *Lett* **37**, 6–11.
- 1477 Chang W. L., Smith R. B., Wicks C., Farrell J. M. and Puskas C. M. (2007) Accelerated uplift 1478 and magmatic intrusion of the Yellowstone caldera, 2004 to 2006. *Science* (1979) **318**, 952– 1479 956.
- 1480 Cheng H., Lawrence Edwards R., Shen C. C., Polyak V. J., Asmerom Y., Woodhead J.,
- Hellstrom J., Wang Y., Kong X., Spötl C., Wang X. and Calvin Alexander E. (2013)
- Improvements in ²³⁰Th dating, ²³⁰Th and ²³⁴U half-life values, and U-Th isotopic
- measurements by multi-collector inductively coupled plasma mass spectrometry. *Earth*
- 1484 *Planet Sci Lett* **371–372**, 82–91.

1472

- 1485 Ciraula D. A., Carr B. J. and Sims K. W. W. (2023a) Geophysical Imaging of the Shallow
 1486 Geyser and Hydrothermal Reservoir Structures of Spouter Geyser, Yellowstone National
 1487 Park: Geyser Dynamics I. *J Geophys Res Solid Earth* 128.
- 1488 Ciraula D. A., Carr B. J. and Sims K. W. W. (2023b) Time-Lapse Geophysical Investigation of 1489 Geyser Dynamics at Spouter Geyser, Yellowstone National Park: Geyser Dynamics II. *J* 1490 *Geophys Res Solid Earth* **128**.
- 1491 Clark J. F. and Turekian K. K. (1990) Time scale of hydrothermal water-rock reactions in Yellowstone National Park based on radium isotopes and radon. *J Volcanol Geotherm Res* 40, 169–180.
- 1494 Colman D. R., Amenabar M. J., Fernandes-Martins M. C. and Boyd E. S. (2022) Subsurface
 1495 Archaea associated with rapid geobiological change in a model Yellowstone hot spring.
 1496 Commun Earth Environ 3.
- 1497 Colman D. R., Feyhl-Buska J., Robinson K. J., Fecteau K. M., Xu H., Shock E. L. and Boyd E.
 1498 S. (2016) Ecological differentiation in planktonic and sediment-associated chemotrophic
 1499 microbial populations in Yellowstone hot springs. *FEMS Microbiol Ecol* **92**, 137.
- Colman D. R., Lindsay M. R., Amenabar M. J. and Boyd E. S. (2019) The Intersection of Geology, Geochemistry, and Microbiology in Continental Hydrothermal Systems. *Astrobiology* **19**, 1505–1522.
- 1503 Colman D. R., Lindsay M. R., Amenabar M. J., Fernandes-Martins M. C., Roden E. R. and Boyd E. S. (2020) Phylogenomic analysis of novel Diaforarchaea is consistent with sulfite but not sulfate reduction in volcanic environments on early Earth. *ISME J* 14, 1316–1331.
- Colman D. R., Lindsay M. R., Harnish A., Bilbrey E. M., Amenabar M. J., Selensky M. J.,
 Fecteau K. M., Debes R. V., Stott M. B., Shock E. L. and Boyd E. S. (2021) Seasonal
 hydrologic and geologic forcing drive hot spring geochemistry and microbial biodiversity.
 Environ Microbiol 23, 4034–4053.
- 1510 Colman D. R., Poudel S., Hamilton T. L., Havig J. R., Selensky M. J., Shock E. L. and Boyd E. S. (2018) Geobiological feedbacks and the evolution of thermoacidophiles. *ISME J* 12, 1512 225–236.
- Colman D. R., Veach A., Stefánsson A., Wurch L., Belisle B. S., Podar P. T., Yang Z.,
 Klingeman D., Senba K., Murakami K. S., Kristjánsson J. K., Björnsdóttir S. H., Boyd E. S.
 and Podar M. (2023) Tectonic and geological setting influence hot spring microbiology. *Environ Microbiol*.
- Doe B. R., Leeman W. P., Christiansen R. L. and Hedge C. E. (1982) Lead and strontium isotopes and related trace elements as genetic tracers in the Upper Cenozoic rhyolite-basalt association of the Yellowstone Plateau Volcanic Field. *J Geophys Res* **87**, 4785–4806.
- Dutton A., Rubin K., McLean N., Bowring J., Bard E., Edwards R. L., Henderson G. M., Reid M. R., Richards D. A., Sims K. W. W., Walker J. D. and Yokoyama Y. (2017) Data reporting standards for publication of U-series data for geochronology and timescale assessment in the earth sciences. *Quat Geochronol* 39, 142–149.
- Edwards K. J., Goebel B. M., Rodgers T. M., Schrenk M. O., Gihring T. M., Cardona M. M., Hu
 B., McGuire M. M., Hamers R. J., Pace N. R. and Banfield J. F. (1999) Geomicrobiology of
 pyrite (FeS₂) dissolution: Case study at iron mountain, California. *Geomicrobiol J* 16, 155–
 179.
- Fernandes-Martins M. C., Colman D. R. and Boyd E. S. (2023) Relationships between fluid mixing, biodiversity, and chemosynthetic primary productivity in Yellowstone hot springs. *Environ Microbiol* **25**, 1022–1040.

- 1531 Fernandes-Martins M. C., Keller L. M., Munro-Ehrlich M., Zimlich K. R., Mettler M. K.,
- England A. M., Clare R., Surya K., Shock E. L., Colman D. R. and Boyd E. S. (2021)
- Ecological dichotomies arise in microbial communities due to mixing of deep hydrothermal waters and atmospheric gas in a circumneutral hot spring. *Appl Environ Microbiol*.
- Fouke B. W., Farmer J. D., Des Marais D. J., Pratt L., Sturchio N. C., Burns P. C. and Discipulo M. K. (2000) Depositional facies and aqueous-solid geochemistry of travertine-depositing hot springs (Angel Terrace, Mammoth Hot Springs, Yellowstone National Park, U.S.A.). *J Sediment Res* **70**, 565–585.
- Fournier R. O. (1979) Geochemical and hydrologic considerations and the use of enthalpychloride diagrams in the prediction of underground conditions in hot-spring systems. *J Volcanol Geotherm Res* **5**, 1–16.
- Fournier R. O. (1989) Geochemistry and Dynamics of the Yellowstone National Park Hydrothermal System. *Annu Rev Earth Planet Sci* **17**, 13–53.
- Fournier R. O., Weltman U., Counce D., White L. D. and Janik C. J. (2002) Results Of Weekly Chemical And Isotopic Monitoring Of Selected Springs In Norris Geyser Basin, Yellowstone National Park During June-September, 1995. U.S. Geological Survey Open File Report 02–344, 50.
- Gardner W Payton, Susong D. D., Solomon D. K. and Heasler H. (2010) Snowmelt hydrograph interpretation: Revealing watershed scale hydrologic characteristics of the Yellowstone volcanic plateau. *J Hydrol (Amst)* **383**, 209–222.
- Gardner W. P., Susong D. D., Solomon D. K. and Heasler H. P. (2011) A multitracer approach for characterizing interactions between shallow groundwater and the hydrothermal system in the Norris Geyser Basin area, Yellowstone National Park. *Geochem Geophys Geosyst* 12, 1–17.
- Gardner W. Payton, Susong D. D., Solomon D. K. and Heasler H. P. (2010) Using noble gases measured in spring discharge to trace hydrothermal processes in the Norris Geyser Basin, Yellowstone National Park, U.S.A. *J Volcanol Geotherm Res* **198**, 394–404.
- Giammanco S. and Sims K. W. W. (2022) Monitoring Volcanic Activity Through Combined

 Measurements of CO₂ Efflux and (²²²Rn) and (²²⁰Rn) in Soil Gas. In *Isotopic Constraints on Earth System processes* pp. 167–202.

 Giammanco S., Sims K. W. W. and Neri M. (2007) Measurements of ²²⁰Rn and ²²²Rn and CO₂
 - Giammanco S., Sims K. W. W. and Neri M. (2007) Measurements of ²²⁰Rn and ²²²Rn and CO₂ emissions in soil and fumarole gases on Mt. Etna volcano (Italy): Implications for gas transport and shallow ground fracture. *Geochem Geophys Geosyst* **8**, 1–14.
- Gibson M. L. and Hinman N. W. (2013) Mixing of hydrothermal water and groundwater near hot springs, Yellowstone National Park (USA): hydrology and geochemistry Matthew. *Hydrogeol J* 21, 919–933.
- Giggenbach W. F. (1988) Geothermal solute equilibria. Derivation of the Na–K–Mg-Ca geoindicators. *Geochim Cosmochim Acta* **52**, 2749–2765.
- Hague A. (1904) Yellowstone National Park. Scribner's Magazine.
- Heasler H. and Jaworowski C. (2018) Hydrothermal monitoring of Norris Geyser Basin,
 Yellowstone National Park, USA, using airborne thermal infrared imagery. Geothermics 72,
- 1572 24-46

1563

Henderson P. B., Morris P. J., Moore W. S. and Charette M. A. (2013) Methodological advances for measuring low-level radium isotopes in seawater. *J Radioanal Nucl Chem.* pp. 357–362.

- Hildreth W., Christiansen R. L. and O'Neil J. R. (1984) Catastrophic Isotopic Modification of Rhyolitic Magma at Times of Caldera Subsidence, Yellowstone Plateau Volcanic Field. *J Geophys Res* **89**, 8339–8369.
- Hildreth W., Halliday A. N. and Christiansen R. L. (1991) Isotopic and Chemical Evidence
 Concerning the Genesis and Contamination of Basaltic and Rhyolitic Magma Beneath the
 Yellowstone Plateau Volcanic Field. *J Petrol* 32, 63–138.
- Holden N. E. (1990) Total Half-Lives for Selected Nuclides. Pure & Appl, Chem 62, 941–958.
- Hou W., Wang S., Dong H., Jiang H., Briggs B. R., Peacock J. P., Huang Q., Huang L., Wu G., Zhi X., Li W., Dodsworth J. A., Hedlund B. P., Zhang C., Hartnett H. E., Dijkstra P. and Hungate B. A. (2013) A Comprehensive Census of Microbial Diversity in Hot Springs of Tengchong, Yunnan Province China Using 16S rRNA Gene Pyrosequencing. *PLoS One* 8.
- von Humboldt A. (1863) *Cosmos: A Sketch of a physical description of the universe.*, Harper & Bros, New York.
- Hurwitz S. and Lowenstern J. B. (2014) Dynamics of the Yellowstone hydrothermal system. *Rev Geophys* **52**, 375–411.
- Inskeep W. P., Jay Z. J., Tringe S. G., Herrgård M. J. and Rusch D. B. (2013) The YNP metagenome project: Environmental parameters responsible for microbial distribution in the yellowstone geothermal ecosystem. *Front Microbiol* **4**.
 - Jaffey A. H., Flynn K. F., Glendenin L. E., Bentley W. C. and Essling A. M. (1971) Precision Measurement of Half-Lives and Specific Activities of ²³⁵U and ²³⁸U. **4**, 1889-1906.

1594

1595 1596

1597

1598

1599

1600

1601

1602

1603

1604

1605

1606

- Jaworowski C., Heasler H. P., Hardy C. C. and Queen L. P. (2006) Control of hydrothermal fluids by natural fractures at Norris Geyser Basin. *Yellowstone Science* **14**, 13–26.
- Jaworowski C., Susong D., Heasler H., Mencin D., Johnson W., Conrey R. and Von Stauffenberg J. (2016) *Geologic and Geochemical Results from Boreholes Drilled in Yellowstone National Park, Wyoming, 2007 and 2008.*
- Kadko D. and Butterfield D. A. (1998) The relationship of hydrothermal fluid composition and crustal residence time to maturity of vent fields on the Juan de Fuca Ridge. *Geochim Cosmochim Acta* **62**, 1521–1533.
- Kadko D., Gronvold K. and Butterfield D. (2007) Application of radium isotopes to determine crustal residence times of hydrothermal fluids from two sites on the Reykjanes Peninsula, Iceland. *Geochim Cosmochim Acta* **71**, 6019–6029.
- Kadko D. and Moore W. (1988) Radiochemical constraints on the crustal residence time of submarine hydrothermal fluids: Endeavour Ridge. *Geochim Cosmochim Acta* **52**, 659–668.
- Kang D. D., Froula J., Egan R. and Wang Z. (2015) MetaBAT, an efficient tool for accurately reconstructing single genomes from complex microbial communities. *PeerJ* 3, e1165.
- Keller G. V. and Frischknecht F. C. (1966) *Electrical methods of geophysical prospecting.*,
 Pergamon Press, Oxford, NY.
- Kharaka Y. K., Mariner R. H., Bullen T. D., Kennedy B. M. and Sturchio N. C. (1991)
 Geochemical investigations of hydraulic connections between the Corwin Springs Known
 Geothermal Resources Area and adjacent parts of Yellowstone., Menlo Park.
- 1615 Kharaka Y. K., Thorsden J. J. and White L. D. (2002) *Isotope and chemical compositions of meteoric and thermal waters and snow from the greater Yellowstone National Park region.*,
- Krishnaswami S., Graustein W. C., Turekian K. K. and Dowd J. F. (1982) Radium, thorium and radioactive lead isotopes in groundwaters: Application to the in situ determination of
- adsorption-desorption rate constants and retardation factors. *Water Resour Res* **18**, 1663–1620 1675.

- Lane-Smith D. and Sims K. W. W. (2013) The Effect of CO₂ on the Measurement of ²²⁰Rn and ²²²Rn with Instruments Utilising Electrostatic Precipitation. *Acta Geophysica* **61**, 822–830.
- Layne G. D. and Sims K. W. (2000) Secondary ion mass spectrometry for the measurement of ²³²Th/²³⁰Th in volcanic rocks. *Int J Mass Spectrom* **203**, 187–198.
- Le Roux L. and Glendenin L. (1963) Half-life of 232Th. In *Proceedings of the National Meeting* on *Nuclear Energy* Pretoria.
- Leeman W. P., Doe B. R. and Whelan J. (1977) Radiogenic and stable isotope studies of hotspring deposits in Yellowstone National Park and their genetic implications. *Geochem J* 11, 65–74.
- Li H. (2015) BFC: Correcting Illumina sequencing errors. *Bioinformatics* **31**, 2885–2887.
- Licciardi J. M. and Pierce K. L. (2018) History and dynamics of the Greater Yellowstone Glacial System during the last two glaciations. *Quat Sci Rev* **200**, 1–33.
- Lowenstern J. B., Bergfeld D., Evans W. C. and Hurwitz S. (2012) Generation and evolution of hydrothermal fluids at Yellowstone: Insights from the Heart Lake Geyser Basin. *Geochem Geophys Geosyst* 13, 1–20.
- McCleskey B. R., Chiu R. B., Nordstrom D. K., Campbell K. M., Roth D. A., Ball J. W. and Plowman T. I. (2014) Water-Chemistry Data for Selected Springs, Geysers, and Streams in Yellowstone National Park, Wyoming, Beginning 2009.
- McCleskey R. B., Ball J. W., Nordstrom D. K., Holloway J. M. and Taylor H. E. (2005) Water-Chemistry Data for Selected Hot Springs, Geysers, and Streams in Yellowstone National Park, Wyoming, 2001-2002. 1–102.
- McCleskey R. B., Nordstrom D. K., Hurwitz S., Colman D. R., Roth D. A., Johnson M. and Boyd E. S. (2022a) The source, fate, and transport of arsenic in the Yellowstone hydrothermal system - An overview. *J Volcanol Geotherm Res* **432**, 107709.
- McCleskey, R.B., Roth, D.A., Nordstrom, D.K., Hurwitz, S., Holloway, J.M., Bliznik, P.A., Ball,
 J.W., Repert, D.A., and Hunt, A.G., (2022b), Water-Chemistry and Isotope Data for
 Selected Springs, Geysers, Streams, and Rivers in Yellowstone National Park, Wyoming:
 U.S. Geological Survey data release, https://doi.org/10.5066/P92XKJU7.
- Meen J. K. and Eggler D. H. (1987) Petrology and geochemistry of the Cretaceous Independence volcanic suite, Absaroka Mountains, Montana: Clues to the composition of the Archean sub-Montanan mantle. *GSA Bulletin* **98**.
- Meyer-Dombard D. R., Shock E. L. and Amend J. P. (2005) Archaeal and bacterial communities in geochemically diverse hot springs of Yellowstone National Park, USA. *Geobiology* **3**, 211–227.
- Meyer-Dombard D. R., Swingley W., Raymond J., Havig J., Shock E. L. and Summons R. E.
 (2011) Hydrothermal ecotones and streamer biofilm communities in the Lower Geyser
 Basin, Yellowstone National Park. *Environ Microbiol* 13, 2216–2231.
- Moore W. S. (2008) Fifteen years experience in measuring ²²⁴Ra and ²²³Ra by delayedcoincidence counting. *Mar Chem* **109**, 188–197.
- Moore W. S. and Arnold R. (1996) Measurement of ²²³Ra and ²²⁴Ra in coastal waters using a delayed coincidence counter. *J Geophys Res Oceans* **101**, 1321–1329.
- Moore W. S. and Cai P. (2013) Calibration of RaDeCC systems for ²²³Ra measurements. *Mar Chem* **156**, 130–137.
- Moore W. S. and Reid D. F. (1973) Extraction of radium from natural waters using manganeseimpregnated acrylic fibers. *J Geophys Res* **78**, 8880–8886.

- Moreras-Marti A., Fox-Powell M., Zerkle A. L., Stueeken E., Gazquez F., Brand H. E. A., Galloway T., Purkamo L. and Cousins C. R. (2021) Volcanic controls on the microbial habitability of Mars-analogue hydrothermal environments. *Geobiology* **19**, 489–509.
- Moriya Y., Itoh M., Okuda S., Yoshizawa A. C. and Kanehisa M. (2007) KAAS: An automatic genome annotation and pathway reconstruction server. *Nucleic Acids Res* **35**, 182–185.
- Mosser J. L., Mosser A. G. and Brock T. D. (1973) Bacterial origin of sulfuric acid in geothermal habitats. *Science* (1979) **179**, 1323–1324.
- Müller-Petke M., Braun M., Hertrich M., Costabel S. and Walbrecker J. (2016) MRSmatlab A software tool for processing, modeling, and inversion of magnetic resonance sounding data. *Geophysics* 81, WB9–WB21.
- Nordstrom D. K., Ball J. W. and McCleskey B. R. (2005) Ground water to surface Water:
 Chemistry of thermal outflows in Yellowstone National Park. In *Geothermal Biology and Geochemistry in Yellowstone National Park*. Montana State University, Bozeman, MT. pp. 73–94.
- Nordstrom D. K., Ball J. W. and McCleskey R. B. (2004) Oxidation reactions for reduced Fe,
 As, and S in thermal outflows in Yellowstone National Park: biotic or abiotic? *Proceedings International Symposium on Water-Rock Interaction* 11, 59–62.
- Nordstrom D. K., McCleskey B. R. and Ball J. W. (2009) Sulfur geochemistry of hydrothermal waters in Yellowstone National Park: IV Acid-sulfate waters. *Appl Geochem* **24**, 191–207.
- Nurk S., Bankevich A., Antipov D., Gurevich A., Korobeynikov A., Lapidus A., Prjibelsky A.,
 Pyshkin A., Sirotkin Y., Stepanauskas R., McLean J., Lasken R., Clingenpeel
 S. R., Woyke T., Tesler G., Alekseyev M. A. and Pevzner P. A. (2013) Assembling
 Genomes and Mini-metagenomes from Highly Chimeric Reads. In *Research in Computational Molecular Biology* (eds. M. Deng, R. Jiang, F. Sun, and X. Zhang). pp. 158–170.
- Oldenburg D. W. and Li Y. (1999) Estimating depth of investigation in dc resistivity and IP surveys. *Geophysics* **64**, 403–416.
- Parks D. H., Imelfort M., Skennerton C. T., Hugenholtz P. and Tyson G. W. (2015) CheckM: assessing the quality of microbial genomes recovered from isolates, single cells, and metagenomes. *Genome Res* **25**, 1043–1055.

 Pasquet S., Holbrook W. S., Carr B. J. and Sims K. W. W. (2016) Geophysical imaging of

- Pasquet S., Holbrook W. S., Carr B. J. and Sims K. W. W. (2016) Geophysical imaging of shallow degassing in a Yellowstone hydrothermal system. *Geophys Res Lett* **43**, 12,027-12,035.
- Payne D., Dunham E. C., Mohr E., Miller I., Arnold A., Erickson R., Fones E. M., Lindsay M. R., Colman D. R. and Boyd E. S. (2019) Geologic legacy spanning >90 years explains unique Yellowstone hot spring geochemistry and biodiversity. *Environ Microbiol* 21, 4180–4195.
- Pearson F. J. and Truesdell A. H. (1978) Tritium in the Waters of Yellowstone National Park. In
 Short Papers of the Fourth International Conference, Geochronology, Cosmochronology,
 Isotope Geology (ed. R. E. Zartman). U.S. Geological Survey, Aspen, CO. pp. 327–329.
- Power J. F., Carere C. R., Lee C. K., Wakerley G. L. J., Evans D. W., Button M., White D.,
 Climo M. D., Hinze A. M., Morgan X. C., McDonald I. R., Cary S. C. and Stott M. B.
 (2018) Microbial biogeography of 925 geothermal springs in New Zealand. *Nat Commun* 9.
- 1709 Richmond G. M. and Waldrop H. A. (1975) Surficial geologic map of the Norris Junction 1710 Quadrangle, Yellowstone National Park, Wyoming.

- 1711 Rodriguez-R L. M., Gunturu S., Tiedje J. M., Cole J. R. and Konstantinidis K. T. (2018)
- Nonpareil 3: Fast Estimation of Metagenomic Coverage and Sequence Diversity. *mSystems* 3.
- Ruppel E. T. (1972) Geology of pre-Tertiary rocks in the northern part of Yellowstone National
 Park, Wyoming, with a section on Tertiary laccoliths, sills, and stocks in and near the
 Gallatin Range, Yellowstone National Park.,
- Ryan W. B. F., Carbotte S. M., Coplan J. O., O'Hara S., Melkonian A., Arko R., Weissel R. A.,
 Ferrini V., Goodwillie A., Nitsche F., Bonczkowski J. and Zemsky R. Global Multi Resolution Topography (GMRT) synthesis data set. *Geochem Geophys Geosyst* 10.
- Rye R. O. and Truesdell A. H. (2007) The Question of Recharge to the Deep Thermal Reservoir
 Underlying the Geysers and Hot Springs of Yellowstone National Park. In *Integrated*Geoscience Studies in the Greater Yellowstone Area Volcanic, Tectonic, and
 Hydrothermal Processes in the Yellowstone Geoecosystem (ed. L. A. Morgan). U.S.
 Geological Survey. pp. 236–270.
- Rye R. O. and Truesdell A. H. (1993) *The question of recharge to the geysers and hot springs of Yellowstone National Park.*
- 1727 Schlundt H. and Breckenridge G. F. (1938) Radioactivity of the Thermal Waters, Gases, and
 1728 Deposits of Yellowstone National Park. *Bulletin of the Geological Society of America* **9**,
 1729 525–538.
- 1730 Schlundt H. and Moore R. B. (1909) Radioactivity of the Thermal Waters of Yellowstone 1731 National Park. *USGS Bulletin* **395**, 1–36.
- Scott S. R., Sims K. W. W., Reagan M. K., Ball L., Schwieters J. B., Bouman C., Lloyd N. S., Waters C. L., Standish J. J. and Tollstrup D. L. (2019) The application of abundance sensitivity filters to the precise and accurate measurement of uranium series nuclides by plasma mass spectrometry. *Int J Mass Spectrom* **435**, 321–332.
- 1736 Seemann T. (2014) Prokka: Rapid prokaryotic genome annotation. *Bioinformatics* **30**, 2068–1737 2069.
- 1738 Shock E. L. and Holland M. E. (2007) Quantitative Habitability. *Astrobiology* 7, 839–851.
- Shock E. L., Holland M., Meyer-Dombard D., Amend J. P., Osburn G. R. and Fischer T. P. (2010) Quantifying inorganic sources of geochemical energy in hydrothermal ecosystems, Yellowstone National Park, USA. *Geochim Cosmochim Acta* 74, 4005–4043.
- Sims K. W. W., Gill J. B., Dosseto A., Hoffmann D. L., Lundstrom C. C., Williams R. W., Ball L., Tollstrup D., Turner S., Prytulak J., Glessner J. J. G., Standish J. J. and Elliot T. (2008a) An inter-laboratory assessment of the thorium isotopic composition of synthetic and rock reference materials. *Geostand Geoanal Res* 32, 65–91.
- 1746 Sims K. W. W. and Hart S. R. (2006) Comparison of Th, Sr, Nd and Pb isotopes in oceanic 1747 basalts: Implications for mantle heterogeneity and magma genesis. *Earth Planet Sci Lett* 1748 **245**, 743–761.
- Sims K. W. W., Hart S. R., Reagan M. K., Blusztajn J., Staudigel H., Sohn R. A., Layne G. D.,
 Ball L. A. and Andrews J. (2008b) ²³⁸U-²³⁰Th-²²⁶Ra-²¹⁰Pb-²¹⁰Po, ²³²Th-²²⁸Ra, and ²³⁵U Pa constraints on the ages and petrogenesis of Vailulu'u and Malumalu lavas, Samoa.
 Geochem Geophys Geosyst 9.
- Sims K. W. W., Maclennan J., Blichert-Toft J., Mervine E. M., Blusztajn J. and Grönvold K. (2013) Short length scale mantle heterogeneity beneath Iceland probed by glacial
- modulation of melting. Earth Planet Sci Lett **379**, 146–157.

- Sims K. W. W., Stark G. J. and Reagan M. K. (2021) An Essential Quaternary Clock for Earth System Sciences: An Overview of the Theory and Applications of U and Th Decay Series Isotopes for the Dating of Young Igneous and Sedimentary Rocks. In *Encyclopedia of* Geology Elsevier. pp. 76–100.
- Smeltz N. Y., Sims K. W. W., Carr B. J. and Parsekian A. D. (2022) Geologic controls on
 hydrothermal groundwater mixing in Yellowstone National Park. *J Volcanol Geotherm Res* 431.
- Stauffer R. E. and Thompson J. M. (1984) Arsenic and antimony in geothermal waters of Yellowstone National Park, Wyoming, USA. *Geochim Cosmochim Acta* **48**, 2547–2561.
- Sturchio N., Bohlke J. and Markun F. (1993) Radium isotope geochemistry of thermal waters, Yellowstone National Park, Wyoming, USA. *Geochim Cosmochim Acta* **57**, 1203–1214.
- Swallow E. J., Wilson C. J. N., Charlier B. L. A. and Gamble J. A. (2018) Mafic inputs into the rhyolitic magmatic system of the 2.08 Ma Huckleberry Ridge eruption, Yellowstone. *Am Mineral* **103**, 757–775.
- Thirlwall M. F. (2002) Multicollector ICP-MS analysis of Pb isotopes using a ²⁰⁷pb-²⁰⁴pb double spike demonstrates up to 400 ppm/amu systematic errors in Tl-normalization. *Chem Geol* **184**, 255–279.
- 1773 Truesdell A. H. and Fournier R. O. (1976) Conditions in the deeper parts of the hot spring systems of Yellowstone National Park.
- 1775 Tuli J. K. (2004) Nuclear Wallet Cards for Radioactive Nuclides., Upton, NY.
- 1776 Uritskiy G. V., DiRuggiero J. and Taylor J. (2018) MetaWRAP—a flexible pipeline for genome-1777 resolved metagenomic data analysis. *Microbiome* **6**, 1–13.
- Valentine D. L. (2007) Adaptations to energy stress dictate the ecology and evolution of the Archaea. *Nat Rev Microbiol* **5**, 316–323.
- Vitale M. V., Gardner P. and Hinman N. W. (2008) Surface water-groundwater interaction and chemistry in a mineral-armored hydrothermal outflow channel, Yellowstone National Park, USA. *Hydrogeol J* 16, 1381–1393.
- Walsh D. O. (2008) Multi-channel surface NMR instrumentation and software for 1D/2D groundwater investigations. *J Appl Geophy* **66**, 140–150.
- Ward L., Taylor M. W., Power J. F., Scott B. J., McDonald I. R. and Stott M. B. (2017)
 Microbial community dynamics in Inferno Crater Lake, a thermally fluctuating geothermal spring. *ISME J* 11, 1158–1167.
- White D. E. (1957) Thermal waters of volcanic origin. *Bulletin of the Geological Society of America* **68**, 1637–1658.
- White D. E., Fournier R. O., Muffler L. J. P. and Truesdell A. H. (1975) Physical Results of
 Research Drilling in Thermal Areas of Yellowstone National Park, Wyoming.,
- White D. E., Heropoulos C. and Fournier R. O. (1992) Gold and other minor elements
 associated with the hot springs and geysers of Yellowstone National Park, Wyoming,
 supplemented with data from Steamboat Springs, Nevada., U.S. Geological Survey.
- White D. E., Hutchinson R. A. and Keith T. E. C. (1988) *The Geology and Remarkable Thermal Activity of Norris Geyser Basin, Yellowstone National Park, Wyoming.*,
- Wu Y.-W., Tang Y.-H., Tringe S. G., Simmons B. A. and Singer S. W. (2014) MaxBin: an automated binning method to recover individual genomes from metagenomes using. *Microbiome* 2, 4904–4909.
- 1800 Xu Y. and Schoonen M. A. A. (1995) The stability of thiosulfate in the presence of pyrite in low-temperature aqueous solutions. *Geochim Cosmochim Acta* **59**, 4605–4622.

1804

Table 1. Isotopic Compositions of hot springs measured at UW.

Location/Sample	Collection Date	δ ⁵⁶ Fe		δ^{57} Fe		$^{87}{\rm Sr}/^{86}{\rm Sr}$		$^{143}Nd/^{144}Nd$		208 Pb/ 206 Pb		$^{207} Pb / ^{206} Pb$	
		ratio	+/-	ratio	+/-	ratio	+/-	ratio	+/-	ratio	+/-	ratio	+/-
Perpetual Spouter													
140724_NGB_PS	7/24/14	0.427	0.044	0.663	0.048	0.711097	0.000009	0.51215	0.00009	2.10357	0.00014	0.85664	0.00004
140917_NGB_PS	9/17/14	-	_	_	-	-	-	-	-	-	-	-	-
150814_NGB_PS	8/14/15	0.525	0.078	0.820	0.131	0.711094	0.000010	0.51207	0.00003	2.1153	0.0005	0.8631	0.0002
170915_NGB_PS	9/15/17	0.639	0.053	0.859	0.133	0.711064	0.000009	0.51235	0.00006	2.1099	0.0005	0.8591	0.0003
Red Bubbler													
140724_NGB_AP	7/24/14	0.332	0.035	0.584	0.025	0.711209	0.000008	0.512177	0.000006	2.21987	0.00003	0.89930	0.00001
140917_NGB_AP	9/17/14	-	_	_	-	-	-	-	-	-	-	-	-
150814_NGB_AP	8/14/15	0.391	0.027	0.627	0.035	0.711201	0.000009	0.512158	0.000003	2.21886	0.00004	0.89900	0.00001
170915_NGB_AP	9/15/17	0.303	0.059	0.452	0.063	0.711141	0.000008	0.512160	0.000005	2.21903	0.00002	0.89918	0.00001
Lower Amphitheater Springs													
140725_AS_LAS	9/17/10	-	-	-	-	0.709375	0.000009	0.512145	0.000006	2.218	-	0.899035183	-
150814_AS_LAS	9/17/10	-	-	-	-	0.709434	0.000007	0.512143	0.000006	2.219	-	0.899353222	-
<u>Lobster Claw</u>													
150718_SS_LC	7/18/15	-	-	-	-	0.711053	0.000007	0.512230	0.000005	2.212	-	0.896066971	-
Echinus Geyser													
141107_NGB_EG	11/7/14	-	-	-	-	0.710719	0.000011	0.512113	0.000005	2.210		0.895646684	
Beryl Spring													
141106_GC_BS	9/22/10	-	-	-	-	0.709367	0.000008	0.513103	0.000505	2.08	-	0.845578514	-
Boiling River													
141108_MT_BR (1)	6/30/10	-	-	-	-	0.710884	0.000008	0.511441	0.000517	2.0688	-	0.84063144	-
141108_MT_BR (2)	6/30/10	-	-	-	-	0.710896	0.000008	-	-	2.0695	-	0.840967241	-
Narrow Gauge													
141108_MT_NG	9/24/10					0.711064	0.000009	-	-	2.078089494	-	0.850769035	-

Errors represent 2SE internal instrument precisions. See Supplemental Material C Table 5 for Compilation of QA reference materials measured during Isotopic Analyses

Table 2. U- and Th-decay series activities and activity ratios.

Location		Perpetual Spouter (44° 43' 35.7276" N, 110° 42' 32.994" W)									ıbbler (44°	43' 35.338	88 N, 110° 4	2' 33.268	B" W)	
Sample	140724_	NGB_PS	140917_NGB_PS 17-Sep-14		150814	150814_NGB_PS		170915_NGB_PS		NGB_AP	140917_NGB_AP		150814_NGB_AP		170915_N	NGB_AF
Date	24-Ju	ıl-14			14-Aug-15		15-Sep-17		24-Jul-14		17-Sep-14		14-Aug-15		15-Sep-17	
	ratio	+/-	ratio	+/-	ratio	+/-	ratio	+/-	ratio	+/-	ratio	+/-	ratio	+/-	ratio	+/-
$(^{224}Ra/^{223}Ra)^{a}$	17.89	3.78	16	4	-	-	-	-	34.9	5.1	41.4	6	-	-	-	-
$(^{224}Ra/^{228}Ra)^{a}$	2.19	0.40	1.9	0.2	-	-	-	-	1.50	0.2	1.4	0.09	-	-	-	-
$(^{228}Ra/^{226}Ra)^{a,b}$	7.01 ^a	1.89	2.5	0.5	8.41 ^b	0.45	-	-	46.9ª	7.1	50.3	0.002	37.9 ^b	0.6	-	-
$(^{230}Th/^{232}Th)^{b}$	-	-	-	-	-	-	-	-	-	-	-	-	0.570	0.001	0.577	0.001
$(^{234}\mathrm{U}/^{238}\mathrm{U})^{\mathrm{b}}$	-	-	-	_	-	-	_	-	-	-	_	-	1.007	0.001	1.008	0.001
$(^{232}\text{Th}/^{238}\text{U})$	-	-	_	_	0.056	0.024	0.100	0.042	-	-	_	-	0.837	0.355	1.211	0.514
$(^{226}Ra/^{222}Rn)^a$	0.002	0.0006	0.0098	0.003	-	-	_	-	0.012	0.00275	0.012	0.0016	-	-	-	_
$(^{224}Ra/^{222}Rn)^a$	0.04	0.006	0.046	0.012	-	-	-	-	0.85	0.18	0.823	0.100	-	-	-	-
	activitya	+/-	activitya	+/-	activityb	+/-	activityb	+/-	activitya	+/-	activitya	+/-	activityb	+/-	activityb	+/-
²²² Rn [dpm/L]	89	6	42	11	-	-	-	-	80	14	70	8	-	-	-	_
²²³ Ra [dpm/L]	0.18	0.03	0.12	0.03	-	-	-	-	2.0	0.2	1.39	0.18	-	-	-	-
²²⁴ Ra [dpm/L]	3.3	0.5	1.9	0.1	-	-	-	-	68.4	8.0	57.60	2.30	-	-	-	-
²²⁶ Ra [dpm/L]	0.21	0.05	0.41	0.07	0.19	0.06	-	-	0.97	0.14	0.83	0.06	1.16	0.35	-	-
²²⁸ Ra [dpm/L]	1.49	0.14	1.01	0.12	1.62	0.49	-	-	45.6	2.3	41.72	2.09	45.9	13.8	-	-
²³⁰ Th [dpm/L]	-	-	-	-	-	-	-	-	-	-	-	-	0.12	0.04	0.13	0.04
ւս լաթուն		-	-	-	0.0001	0.00003	0.0002	0.00006	-	-	-	-	0.22	0.06	0.23	0.07
	-								1							
²³² Th [dpm/L] ²³⁴ U [dpm/L]	-	-	-	-	-	-	-	-	-	-	-	-	0.26	0.08	0.19	0.06

^a Activities measured by decay counting methods

Activity ratios were calculated using λ_{230} =9·195 10⁻⁶ yr⁻¹, λ_{234} = 2·823 10⁻⁶ yr⁻¹, λ_{238} = 1·551 10⁻¹⁰ yr⁻¹; λ_{232} = 4·948 10⁻¹¹ yr⁻¹; λ_{226} = 4·331⁻⁴ yr⁻¹; λ_{228} = 1.201⁻¹ yr⁻¹. (Le Roux & Glendenin, 1963; Jaffey et al., 1971; Holden, 1990; Cheng et al., 2013; Tuli, 2000). Errors (2s) are calculated using standard error propagation methods and include uncertainties in: (1) the decay constants,; (2) the time-averaged uncertainty in spikes used for isotope dilution; (3) the instrument parameters, including the uncertainty in determining the tailing of ²³²Th on ²³⁰Th; (4) the weighing errors; (5) measurement precision for the samples and bracketing standards (0·03–0·4%).

See Scott et al., 2019 and Supplemental Material Table 5 for Compilation of QA reference materials measured during Isotopic Analyses

^b Activities measured by high abundance sensitivity MC-ICPMS mass spectrometry (Scott et al., 2019).

Table 3. Isotopic Compositions of possible aquifer source rocks.

Lithological Unit	Lava Creek Tuff		Huckleberry Ridge Tuff		Lava Creek Tuff A		Lava Creek Tuff B		Lava Creek Tuff A	Lava Creek Tuff B	Lava Creek Tuff A			Lava Creek Tuff B		
Sample	44°38'57" N,	110°47'31" W	44°56'2" N, 1	l10°43'26" W	8YC-4	113	9YC-520)A	8YC-413	65YR-27A	9YC-520A-KF	68-0-49-KF	6YC-146WR (glassy)	6YC-137WR (devit.)	8YC- 413KF	68-0- 48KF
Reference	UW	+/-	uw	+/-	Hildreth, 1991	+/- 2σ	Hildreth, 1991	+/- 2σ	Hildreth e	t al., 1984			Doe et al., 19	982		
δ ⁵⁶ Fe	0.261	0.037	0.706	0.023	-	-	-	-	-	-	-	-	-	-	-	-
δ ⁵⁷ Fe	0.354	0.045	1.030	0.066	-	-	-	-	-	-	-	-	-	-	-	-
⁸⁷ Sr/ ⁸⁶ Sr	-	-	-	-	0.71393	0.00008	0.71012	0.00003	-	-	0.7099	0.7100	0.7109	-	-	0.7099
¹⁴³ Nd/ ¹⁴⁴ Nd	-	-	-		0.512154	0.000019	0.512237	0.000019	-	-	-	-	-	-	-	-
²⁰⁸ Pb/ ²⁰⁶ Pb	-	-	-		-	-	-	-	-	-	2.2218	-	2.223	2.224	2.2297	-
²⁰⁷ Pb/ ²⁰⁶ Pb	-	-	-	-	-	-	-	-	-	-	0.89953	-	0.8989	0.9005	0.89991	-
U (μg/g)	4.57	0.05	1.36	0.01	-	-	5.5	-	12.0	4.5	-	-	6.55	5.88	-	-
Th (μg/g)	24.90	0.2	24.84	0.2	-	-	26.9	-	37.5	25.3	-	-	30.0	28.3	-	-
²²⁶ Ra (fg/g)	1706	20	461.9	6	-	-	-	-	-	-	-	-	-	-	-	-
²³⁸ U (dpm/g) ²³² Th	3.383	0.03	1.01	0.01	-	-	4.1	-	8.89	3.3	-	-	4.85	4.36	-	-
(dpm/g)	6.080	0.06	6.07	0.06	-	-	6.57	-	9.16	6.18	-	-	7.32	6.91	-	-
(²³² Th/ ²³⁸ U) ²²⁶ Ra	1.797	0.018	6.021	0.060	-	-	1.6	-	1.03	1.9	-	-	1.51	1.59	-	-
(dpm/g)	3.742	0.045	1.013	0.012	-	-	-	-	-	-	-	-	-	-	-	-
(²²⁸ Ra/ ²²⁶ Ra)	-	-			-	-	-	-	-	-	-	-	-	-	-	-

Lithological Unit Sample Reference	Averag Average LCT	e LCT 1 SD	Mississippian Mission Canyon Limestone (Devils Slide)	Paleozoio Pennsylvanian Quadrant Sandstone	-Mesozoic Sedimentary Rocks Jurassic Ellis Group (Impure Limestone)	Jurassic Ellis Group (Calcareous Shale) et al., 1993	Cretaceous Cody Shale	Average	Altered Rhyolites Y-12 Drill Core (acid altered)
neierence					Startino	Ct u.i, 1333			
δ ⁵⁶ Fe	-	-	-	-	-	-		-	-
δ ⁵⁷ Fe	-	-	-	-	•	-	-	-	-
⁸⁷ Sr/ ⁸⁶ Sr	0.7108	0.0016	-	-	-	-	-	-	-
$^{143}Nd/^{144}Nd$	-	-	-	-	-	-	-	-	-
208 Pb/ 206 Pb	2.225	0.003	-	-	-	-	_	_	_
$^{207}{Pb}/^{206}{Pb}$	0.900	0.001	-	-	-	-	-	-	-
U (μg/g)	5.4	0.9	1.17	0.62	1.18	0.89	3.40	1.5	1.0
Th (µg/g)	27.1	2	0.03	0.72	1.85	3.21	9.50	3.1	14.5
²²⁶ Ra (fg/g)	-	-	-	-	-		-	-	-
²³⁸ U (dpm/g) ²³² Th	4.0	0.6	0.867	0.46	0.874	0.66	2.52	1.1	0.74
(dpm/g)	6.61	0.5	0.007	0.18	0.452	0.784	2.32	0.75	3.54
$\binom{232}{100}$ Th/ $\binom{238}{100}$ U)	1.7	0.15	0.008	0.38	0.517	1.2	0.921	0.70	4.8
(dpm/g)	1.014	0.012	-	-	-		-	-	-
$(^{228}Ra/^{226}Ra)$	-	-	0.008	0.38	0.52	1.19	0.92	0.60	4.8

Table 3. Isotopic Compositions of possible aquifer source rocks (contd)

Lithological Unit		Madison L	imestone			stone Composite
Sample	7843-L (HC	Cl leachable)	7843-R (7YR-249 (leach)	7YR-249 (residue)	
Reference	UW +/-		UW	+/-	Leeman	et al., 1977
δ ⁵⁶ Fe	-0.758	0.045	-0.307	0.074	-	-
δ ⁵⁷ Fe	-1.100	0.067	-0.483	0.185	-	-
⁸⁷ Sr/ ⁸⁶ Sr	0.709264	0.000010	0.755571	0.000010	-	-
¹⁴³ Nd/ ¹⁴⁴ Nd	0.511926	0.000005	0.511737	0.00009	-	-
$^{208}{\rm Pb}/^{206}{\rm Pb}$	1.71289	0.00003	1.86622	0.00003	2.011	2.074
²⁰⁷ Pb/ ²⁰⁶ Pb	0.66283	0.00001	0.75555	0.00001	0.8117	0.8289
U (μg/g)	-	-	-		1.40	1.84
Th (μg/g)		-	-	-	1.32	2.90
²²⁶ Ra (fg/g)	-	-	-	-	-	-
²³⁸ U (dpm/g) ²³² Th	-	-	-	-	1.04	1.36
(dpm/g)		-	-	-	0.322	0.708
$\binom{232}{10} \frac{1}{10} \frac{1}{10}$	-	-	-	-	0.311	0.519
(dpm/g)	-	-	-	-	-	-
(²²⁸ Ra/ ²²⁶ Ra)	-	-	-	-	-	-

Errors for radiogenic isotopes and stable Fe represent 2SE internal instrument precisions. 87Sr/86Sr ratios are reported as measured ratios.

Activity ratios were calculated using λ_{230} =9·195 10⁻⁶ yr⁻¹, λ_{234} = 2·823 10⁻⁶ yr⁻¹, λ_{238} = 1·551 10⁻¹⁰ yr⁻¹; λ_{232} = 4·948 10⁻¹¹ yr⁻¹; λ_{226} = 4·331⁻⁴ yr⁻¹; λ_{228} = 1.201⁻¹ yr⁻¹. (Le Roux & Glendenin, 1963; Jaffey et al., 1971; Holden, 1990; Cheng et al., 2013; Tuli, 2000). Errors (2s) are calculated using standard error propagation methods and include uncertainties in: (1) the decay constants,; (2) the time-averaged uncertainty in spikes used for isotope dilution; (3) the instrument parameters, including the uncertainty in determining the tailing of ²³²Th on ²³⁰Th; (4) the weighing errors; (5) measurement precision for the samples and bracketing standards (0·03–0·4%).

See Supplemental Material Table 5 for Compilation of QA materials measured during Isotopic Analyses

N.B Sample *YC-413 was not included in the average for the U and Th concentrations and activities since this sample's values were markedly different than all other measurement.

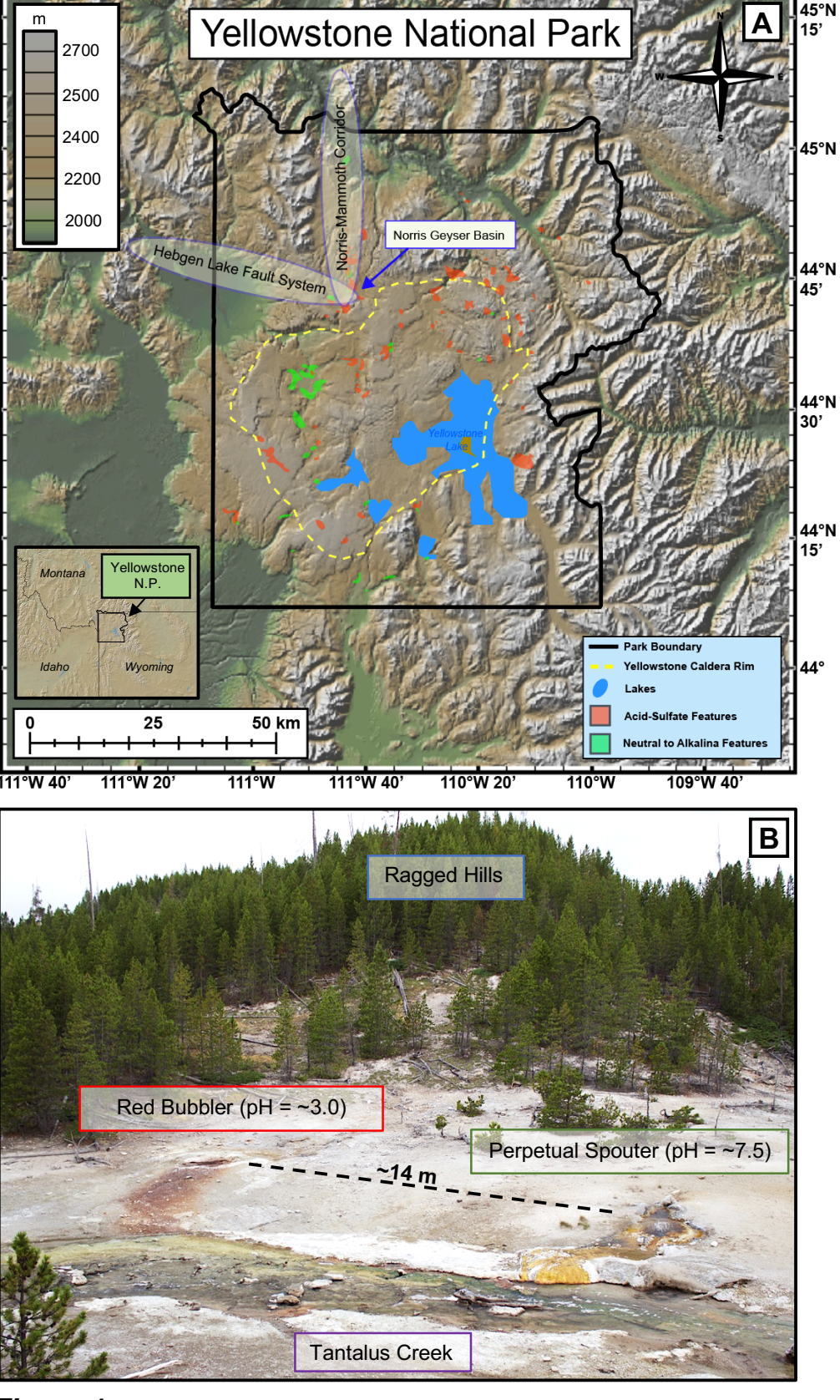
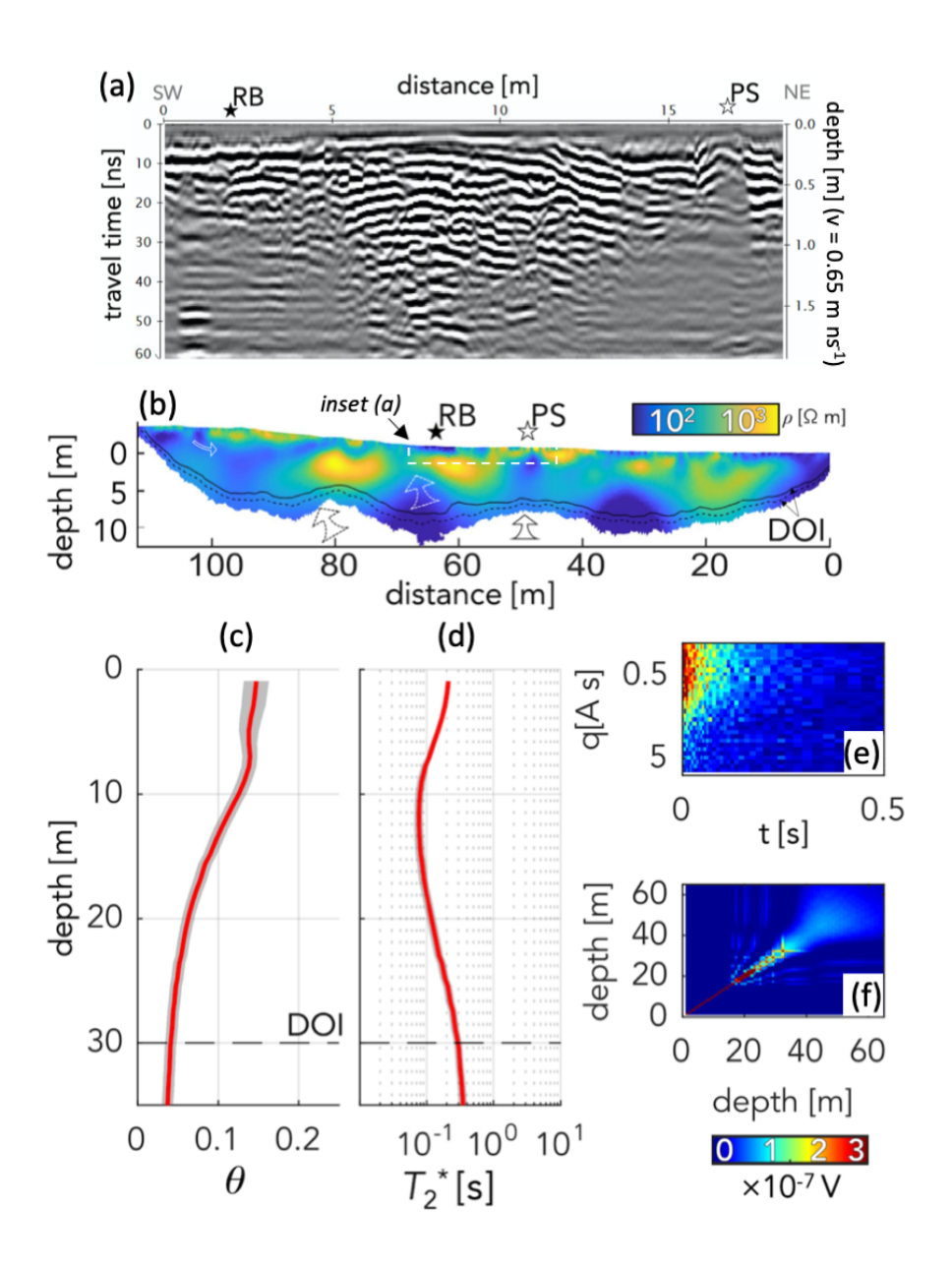
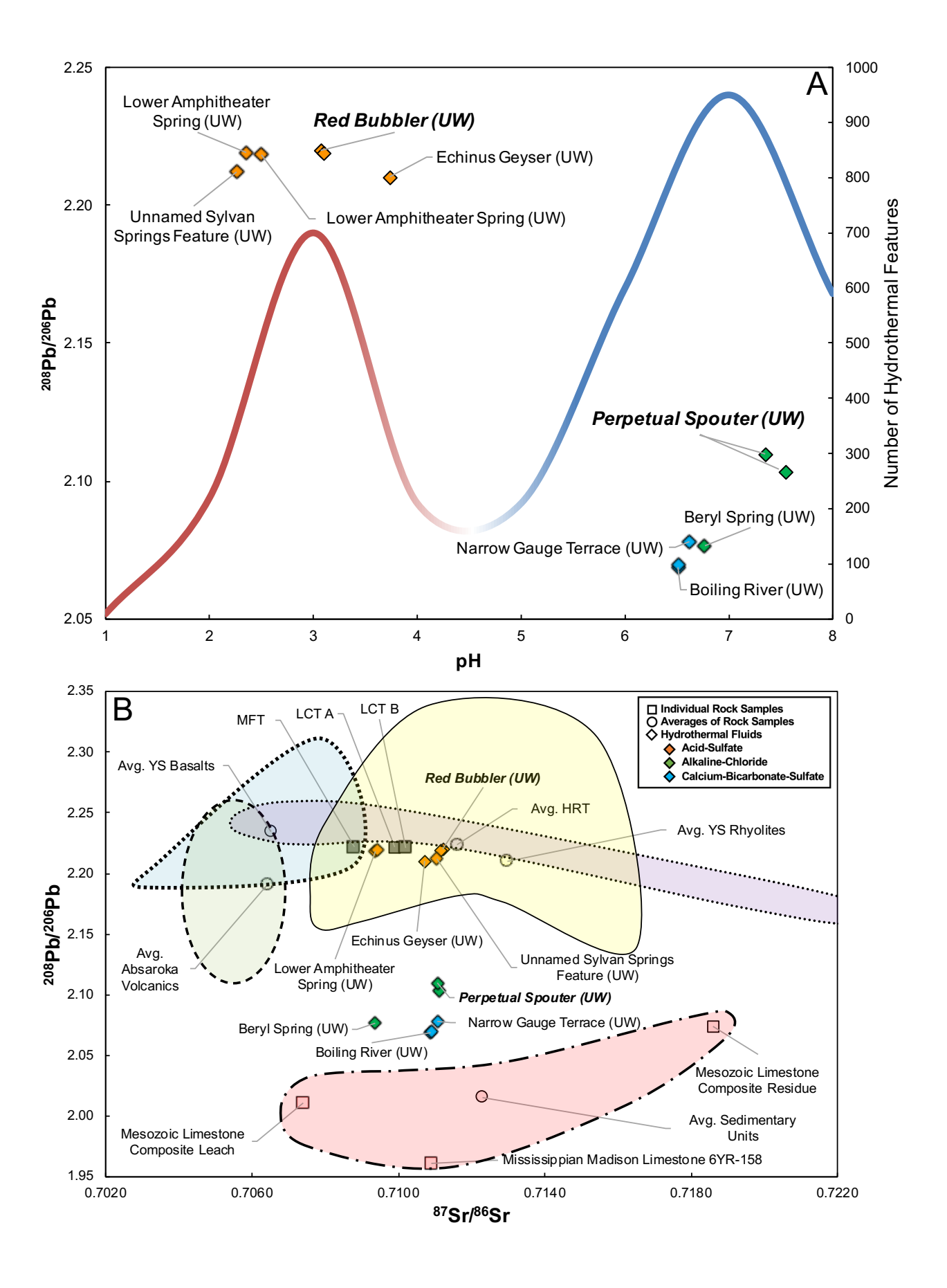
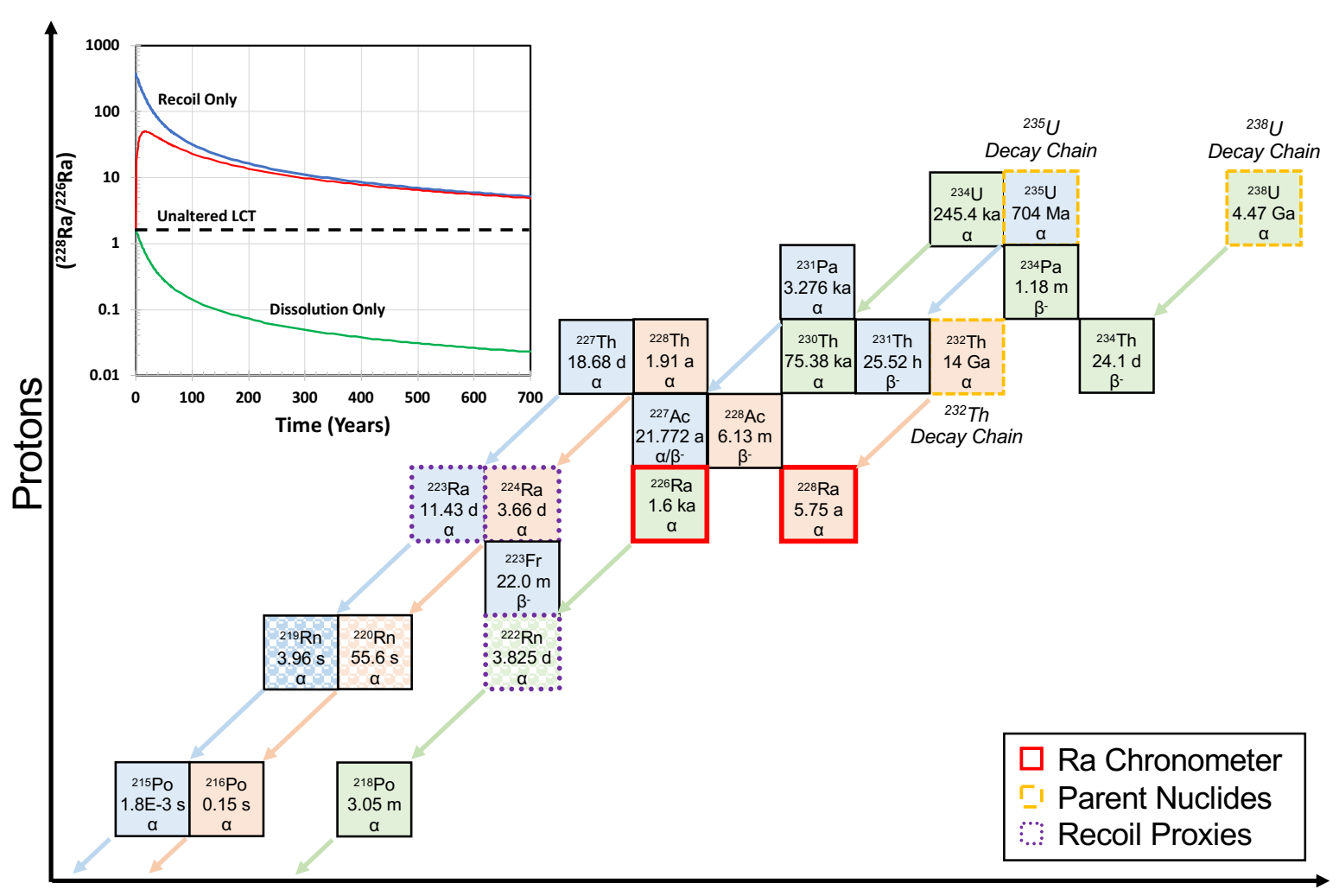


Figure 1







Neutrons

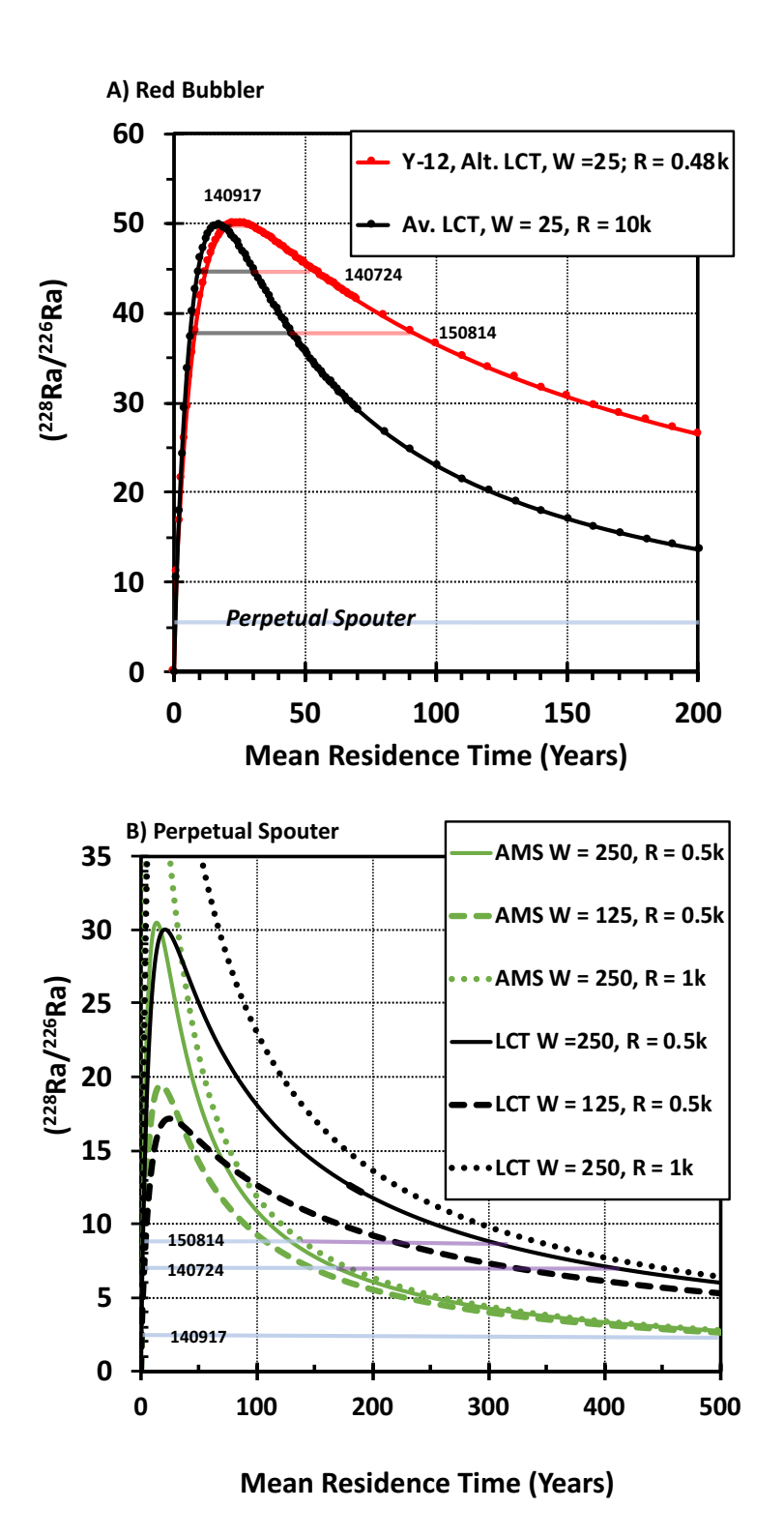
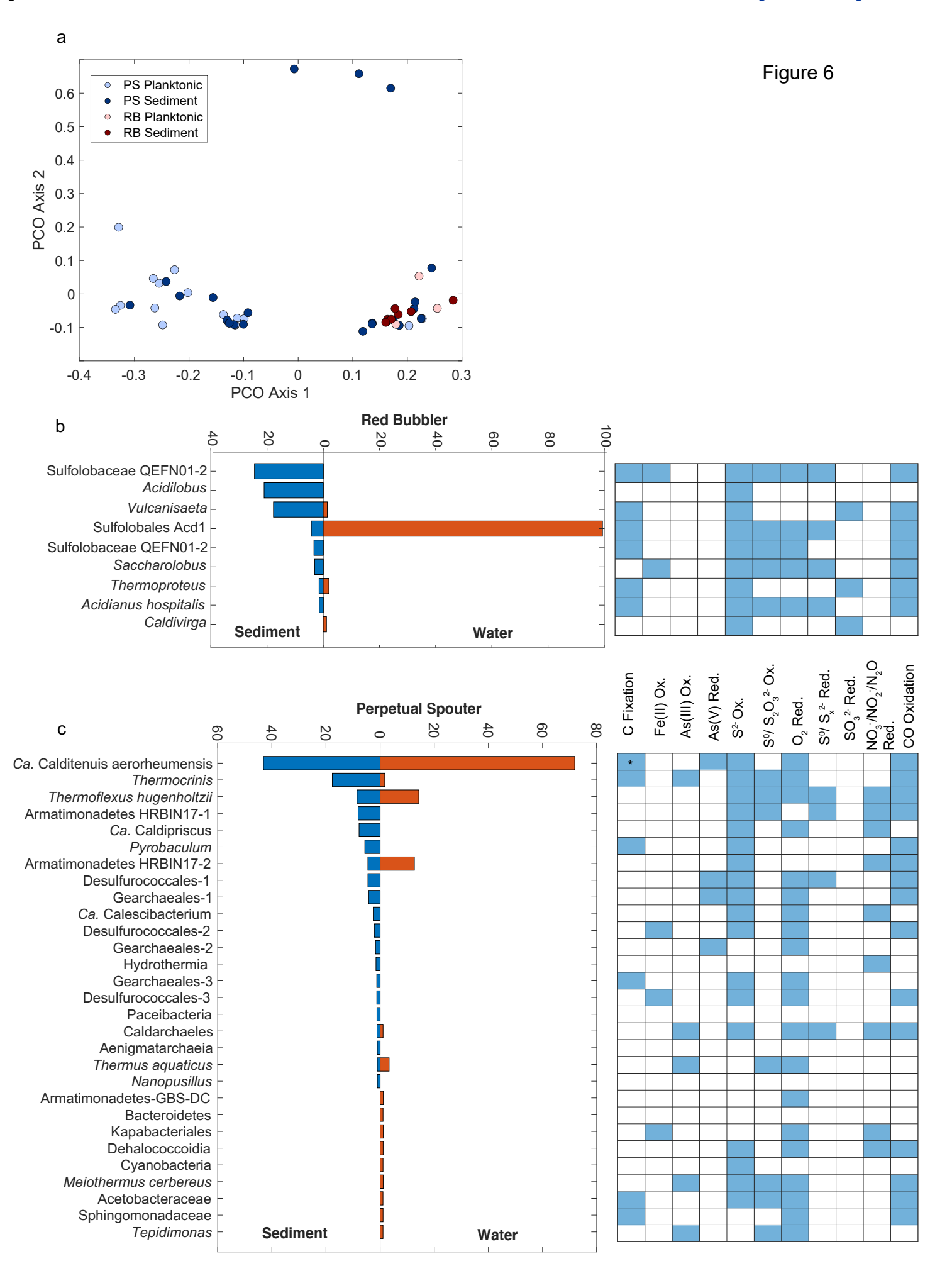
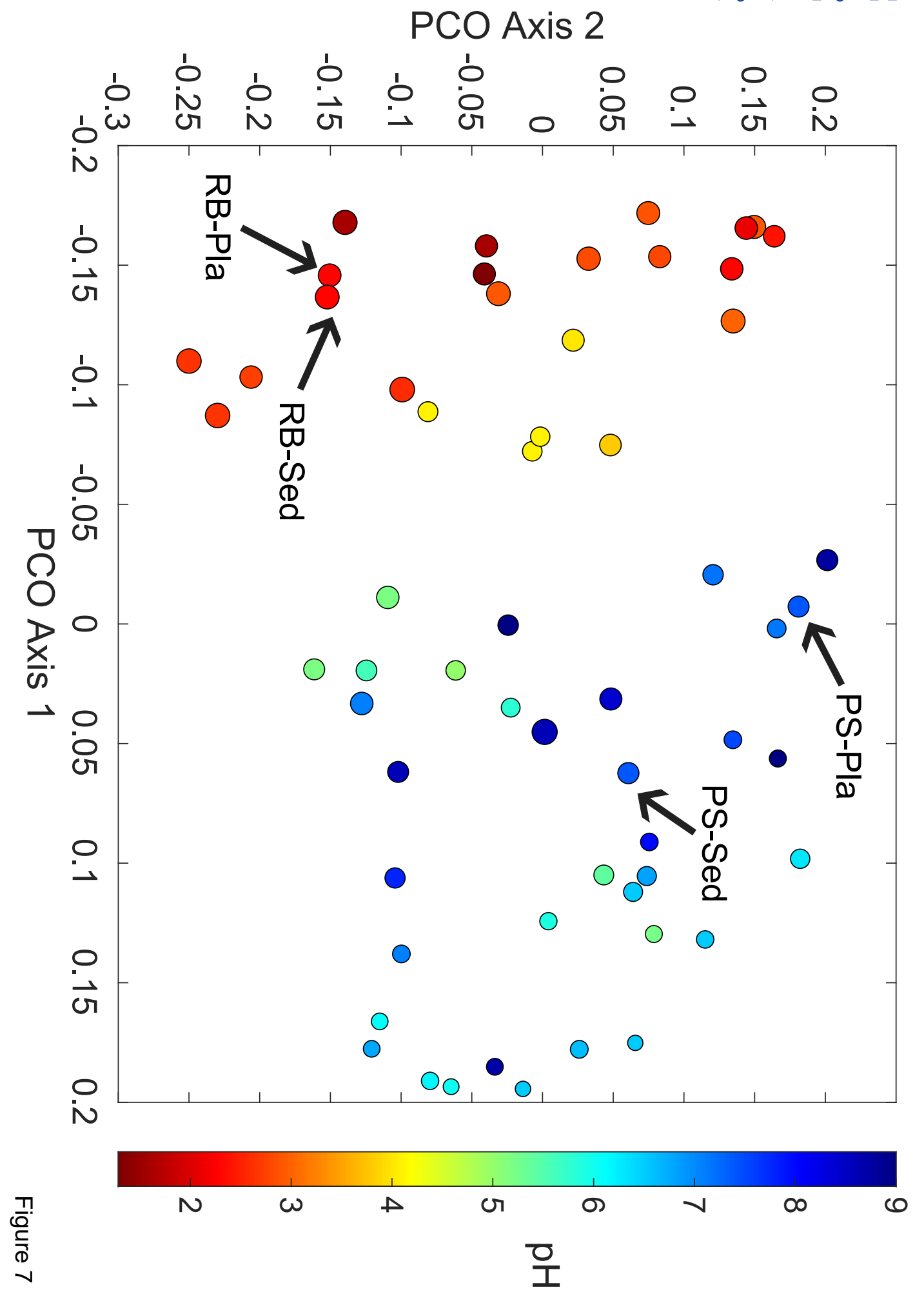


Figure 5





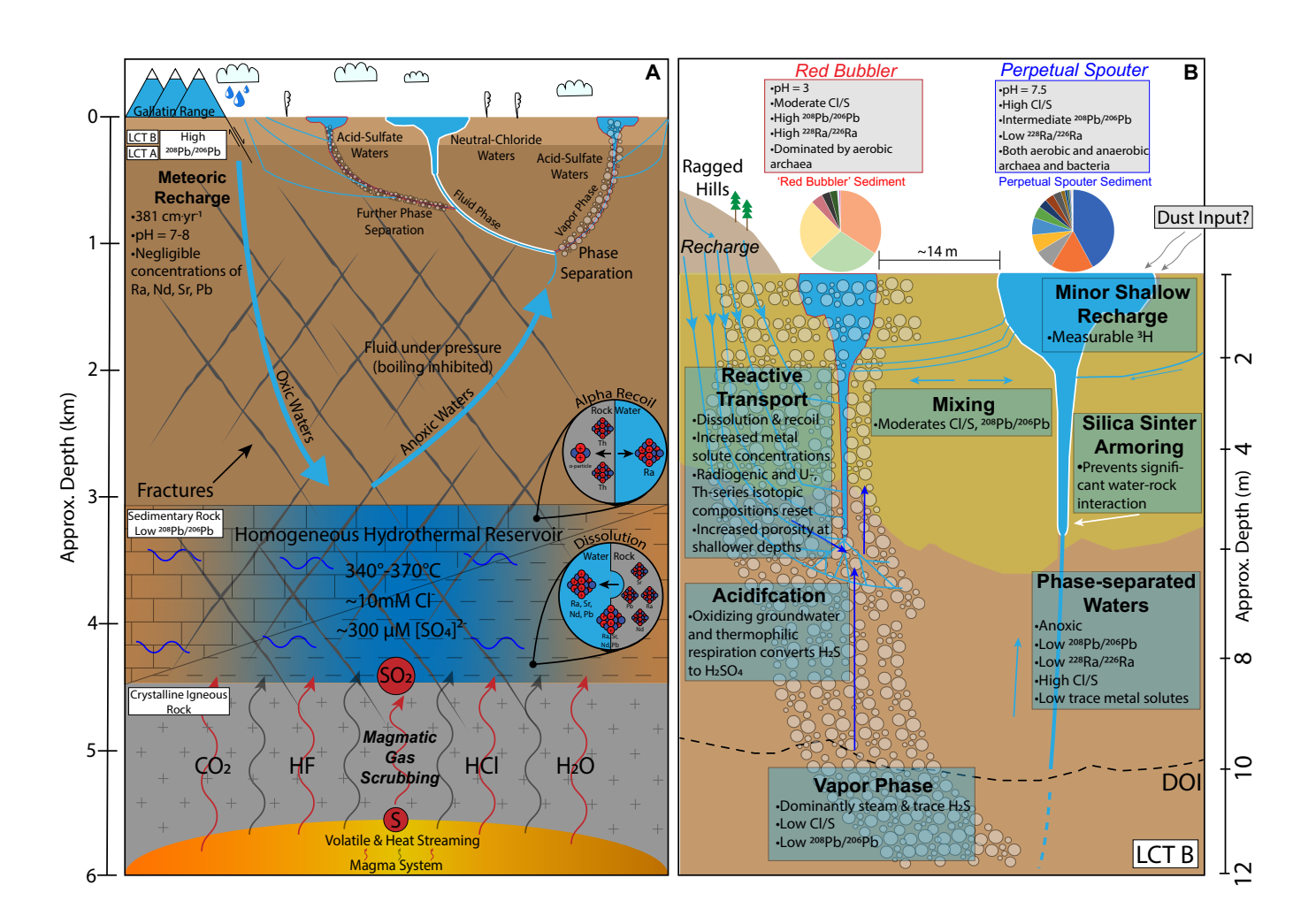


Figure 8